1,3-Ditungstacyclobutadienes. 1. Reactions with Alkynes. Alkyne Adducts and 1,3-Dimetallaallyl Derivatives

Malcolm H. Chisholm,* John C. Huffman, and Joseph A. Heppert

Contribution from the Department of Chemistry and Molecular Structure Center, Indiana University, Bloomington, Indiana 47405. *Received November 27, 1984*

Abstract: $[(Me_3SiCH_2)_2W(\mu\text{-}CSiMe_3)]_2$, **1**, reacts in hydrocarbon solvents with *i*-PrOH to give $[(i\text{-}PrO)_2W(\mu\text{-}CSiMe_3)]_2$, **2**, with elimination of Me_4Si. The molecular structure of **2** is closely related to that of **1** and contains a central $O_4W_2C_2$ unit having virutal D_{2h} symmetry. Pertinent averaged bond distances (angstroms) and angles (degrees) are W-W = 2.62 (1), W-O = 1.85 (1), W-C = 1.90 (5), O-W-O = 115 (1), W-C-W = 86 (1), and C-W-C = 94 (1). Compound **1** reacts in hydrocarbon solutions with alkynes, $R^1C{\equiv}CR^2$, where $R^1 = R^2$ = H, Me, and Ph and R^1 = H and R^2 = Me, Ph, and Me_3Si to give products of insertion of the alkyne into one of the bridging alkylidyne ligands, $W_2(CH_2SiMe_3)_4(\mu\text{-}CSiMe_3)(\mu\text{-}C_3R^1R^2SiMe_3)$. In all cases the reaction proceeds via initial formation of an alkyne adduct which is an intermediate in the insertion reaction. Both the rate of alkyne adduct formation and the rate of insertion are similarly affected by steric factors $k_{RC{\equiv}CH} > k_{RC{\equiv}CR}$. For reactions involving MeC≡CMe and PhC≡CMe, the alkyne adducts have been isolated and characterized. The solid-state molecular structure of $W_2(CH_2SiMe_3)_4(\mu\text{-}CSiMe_3)_2(PhCCMe)$ allows an interpretation of alkyne adduct formation based on a formal oxidative addition wherein the pair of electrons of the M-M bond in **1** is transferred to the alkyne which forms a metallacyclopropene unit: W-W = 2.915 (3) Å, W-C = 2.00 (5) Å, and C-C = 1.30 (5) Å. One tungsten atom is in a pseudotetrahedral geometry forming two W-C single bonds to the CH_2SiMe_3 ligands, W-C = 2.12 (2) Å, and two W-C double bonds, W-C = 1.77 (4) Å (averaged), to the μ-$CSiMe_3$ ligands. The other tungsten atom is in a pseudo-trigonal-bipyramidal geometry if the η^2-alkyne is considered to occupy a single site. The two W-CH_2SiMe_3 ligands, W-C = 2.16 (2) Å (averaged), and one W-μ-$CSiMe_3$ ligand, W-C = 2.15 (3) Å, occupy equatorial sites and the η^2-alkyne and the other μ-$CSiMe_3$ ligand, W-C = 2.19 (4) Å, the axial positions. The other alkyne adducts show NMR spectra interpretable in terms of the adoption of similar structures in solution, and the ^{13}C NMR data for the adduct involving $^*C_2H_2$, where *C represents 92.5 atom % ^{13}C, reveal that the alkyne is acting as a four-electron donor: $\delta(\eta^2\text{-}C_2H_2)$ = 216.8 ppm, $J_{^{183}W\text{-}^{13}C}$ = 33 and $J_{^{13}C\text{-}^{13}C}$ = 42 Hz. Collectively the NMR data indicate that rotation about the alkyne-W vector is rapid on the NMR time scale. A qualitative MO description is presented which accounts for these observations. Studies of the insertion reaction show that the alkyne unit inserts in an intact manner into the μ-$CSiMe_3$ ligand. The migratory insertion reaction is equivalent to a cycloaddition or a ring expansion reaction. Subsequent to the insertion step, rearrangements can occur, scrambling the CR^1, CR^2, and $CSiMe_3$ positions within the μ-C_3 ligand. The reaction between **2** and C_2H_2 proceeds similarly via formation of an ethyne adduct, detectable only at low temperatures (-60 °C), and insertion to give $W_2(O\text{-}i\text{-}Pr)_4(\mu\text{-}CSiMe_3)(\mu\text{-}CHCHSiMe_3)$ which upon heating to +80 °C generates the thermodynamic isomer having a μ-$CHCSiMe_3CH$ ligand. The reaction between **2** and $Me_3SiC{\equiv}CH$ generates initially the $W_2(O\text{-}i\text{-}Pr)_4(\mu\text{-}CSiMe_3)(\mu\text{-}CSiMe_3CHCSiMe_3)$ compound which subsequently rearranges to the isomer containing the μ-$CHCSiMe_3CSiMe_3$ ligand. It is proposed that the insertion step always involves C-C bond formation between the μ-$CSiMe_3$ ligand and the least sterically encumbered carbon atom of the alkyne, but in most instances this is not detected because of subsequent facile site exchange within the μ-C_3 ligand. Rate studies involving the alkyne adducts of **1** and $Me_3SiC{\equiv}CH$ and MeC≡CMe show $\Delta H^\ddagger$ = 15.2 ± 1.2 and 20.5 ± 0.7 kcal mol^{-1}, respectively. The entropies of activation are negative and of medium magnitude, $\Delta S^\ddagger$ = -13 ± 3 eu (MeCCMe) and -15 ± 5 eu (Me_3SiCCH), implying a highly ordered transition state. The μ-C_3 ligand may be viewed as a dimetallated allyl, a 3- ligand, which taken together with the presence of the μ-$CSiMe_3$ ligand, 3-, and four uninegative ligands, CH_2SiMe_3 or O-*i*-Pr, leads to a $(W\text{-}W)^{10+}$ center. The structural characterizations of $W_2(CH_2SiMe_3)_4(\mu\text{-}CSiMe_3)(\mu\text{-}CPhCPhCSiMe_3)$ and $W_2(O\text{-}i\text{-}Pr)_4(\mu\text{-}CSiMe_3)(\mu\text{-}CHCHCSiMe_3)$ reveal W-W distances of 2.548 (1) and 2.658 (1) Å, respectively, consistent with the presence of a W-W bond. In both molecules, one tungsten atom is contained within the μ-C_3 plane of the allyl ligand while the other tungsten atom is π-bonded. The molecules may be viewed as the sum of two fragments: a d^0 $L'L_2W(C_3R_3)$ metallacyclobutadiene unit is π-bonded to a d^2 $L_2L'W$, center, where L = CH_2SiMe_3 or O-*i*-Pr and L′ = μ-$CSiMe_3$. In each molecule, there is a roughly planar X_2WWX_2 unit, where X = C or O, and the $W_2(\mu\text{-}C)$ plane of the alkylidyne ligand is at right angles to the former. Variable-temperature NMR studies reveal a very low-energy process wherein the μ-C_3R_3 ligand flips back and forth between the two tungsten centers. This makes the two tungsten centers equivalent on the NMR time scale, and only for $W_2(O\text{-}i\text{-}Pr)_4(\mu\text{-}CSiMe_3)(\mu\text{-}CHCHCSiMe_3)$ has this been frozen out at low temperatures. The second energy process that is sometimes observed to be rapid on the NMR time scale involves a scrambling of CR sites within the μ-C_3R_3 ligand. This does not involve a reversible deinsertion process. A general scheme for the scrambling of CR positions within the μ-C_3R_3 ligand is proposed based on the reversible formation of a $W_2(\mu\text{-}\eta^1,\eta^2\text{-cyclopropene})$ intermediate by formation of a C-C bond between the α and α' carbon atoms of the allyl moiety. By a sequence of 60 °C rotations followed by ring openings, all possible isomers of the μ-$CR^1CR^2CR^3$ ligand are accessible. These findings are discussed briefly in the context of related findings involving mono-, di-, and trinuclear compounds. The summary of crystal data is as follows: for (i) $W_2(O\text{-}i\text{-}Pr)_4(\mu\text{-}CSiMe_3)_2$ at -69 °C, a = 15.335 (4) Å, b = 11.515 (3) Å, c = 10.652 (3) Å, β = 122.52 (1)°, γ = 99.96 (1)°, Z = 2, d_{calcd} = 1.659 g cm^{-3}, and space group $P\bar{1}$; (ii) for $W_2(CH_2SiMe_3)_4(\mu\text{-}CSiMe_3)_2(\eta^2\text{-}PhCCMe)$ at -157 °C, a = 20.322 (13) Å, b = 12.344 (6) Å, c = 17.936 (10) Å, β = 91.16 (3)°, Z = 4, d_{calcd} = 1.487 g cm^{-3}, and space group $P2_1/a$; for $W_2(CH_2SiMe_3)_4(\mu\text{-}CSiMe_3)(\mu\text{-}CPhCPhCSiMe_3)$ at -160 °C, a = 20.884 (9) Å, b = 13.734 (5) Å, c = 16.842 (6) Å, Z = 4, d_{calcd} = 1.465 g cm^{-3}, and space group $P2_12_12_1$; for $W_2(O\text{-}i\text{-}Pr)_4(\mu\text{-}CSiMe_3)(\mu\text{-}CHCHCSiMe_3)$ at -158 °C, a = 17.827 (7) Å, b = 17.872 (8) Å, c = 10.025 (3) Å, α = 106.07 (2)°, Z = 4, d_{calcd} = 1.732 g cm^{-3}, and space group $P2_1/c$.

Previous work has shown that $W_2(OR)_6(M{\equiv}M)$ compounds react with alkynes to give a variety of products including simple alkyne adducts,[1] having a central pseudotetrahedral M_2C_2 core, and alkylidyne complexes $(RO)_3W{\equiv}CR'$ arising from a metathesis of the W≡W and C≡C bonds.[2] In the case of the compounds $W_2(O\text{-}t\text{-}Bu)_6(py)(\mu\text{-}C_2H_2)$, there is evidence for an equilibrium in toluene solution between the ethyne adduct and

(1) Chisholm, M. H.; Folting, K.; Hoffman, D. M.; Huffman, J. C. *J. Am. Chem. Soc.* **1984**, *106*, 6794.

(2) Schrock, R. R.; Listemann, M. L.; Sturgeoff, L. C. *J. Am. Chem. Soc.* **1982**, *104*, 4291. Schrock, R. R.; Listemann, M. L.; Sturgeoff, L. C. *Organometallics* **1985**, *4*, 69.

0002-7863/85/1507-5116$01.50/0

the methylidyne complex. On the basis of bond distances and small C–C coupling constants, we have formulated the alkyne adducts as dimetallatetrahedranes, I.[1] These observations raise

I

questions concerning the reaction pathway that allows a dimetallatetrahedrane to break apart to two alkylidyne metal fragments and the reverse reaction, yielding M–M and C–C bond formation. Are 1,2-dimetallacyclobutadienes, II, or 1,3-dimetallacyclobutadienes, III, involved?

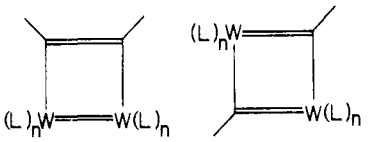

II III

These considerations have led us to turn our attention to the chemistry of tungsten compounds containing a central planar $[MCR]_2$ core.

The occurrence of so-called parallel acetylene compounds is well documented and Hoffmann and Hoffman[3] have discussed the interconversion of perpendicular and parallel acetylene complexes but not specifically for d^3–d^3 dimers. Most, if not all, parallel acetylene complexes are best viewed as 1,2-dimetallacyclobutenes having 10 electrons in the M_2C_2 bonding unit, whereas II represents a 1,2-dimetallacyclobutadiene having a 12-electron M_2C_2 core. To our knowledge, there are no known examples of organometallic compounds which provide bona fide examples of II. However, there is in the literature a series of compounds of formula $[(Me_3SiCH_2)_2M(\mu\text{-}CSiMe_3)]_2$, where M = Nb, Ta,[4] W,[5,6] and Re,[7] which adopt the structure depicted by IV. These are 1,3-dimetallacyclobutadienes of type III with d^0–d^0 (Nb, Ta), d^1–d^1 (W), and d^2–d^2 (Re) metal centers.

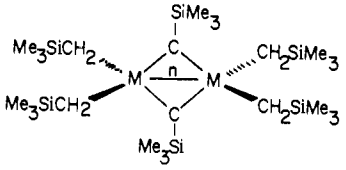

M	n
Ta, Nb	0
W	1
Re	2

IV

In the d^0–d^0 compounds, there is no formal metal–metal bond, whereas for the d^1–d^1 compound, a M–M σ bond can be expected. This is in agreement with the M–M distances of 2.897 (2) and 2.535 (10) Å for M = Nb^V and W^V, respectively. In the case of the d^2–d^2 dimer, a Re–Re double bond might naively be expected, but on the basis of EHMO calculations, a M–M $\sigma^2\delta^{*2}$ configuration is predicted which is consistent with the observation that the Re–Re distance is 2.557 (1) Å,[7] slightly longer than that for the ditungsten compound. The detailed nature of the bonding in these and related 1,3-dimetallacyclobutadienes is currently under investigation and will be discussed at length subsequently.[8]

By controlled alcoholyses (vida infra), we have prepared related $[(RO)_2W(\mu\text{-}CSiMe_3)]_2$ compounds. We are thus in a position to examine the chemistry of compounds containing a planar central $[MCR]_2$ unit, 1,3-dimetallacyclobutadienes, as a function of d^n configuration (d^0–d^0, d^1–d^1, and d^2–d^2) and supporting ligands,

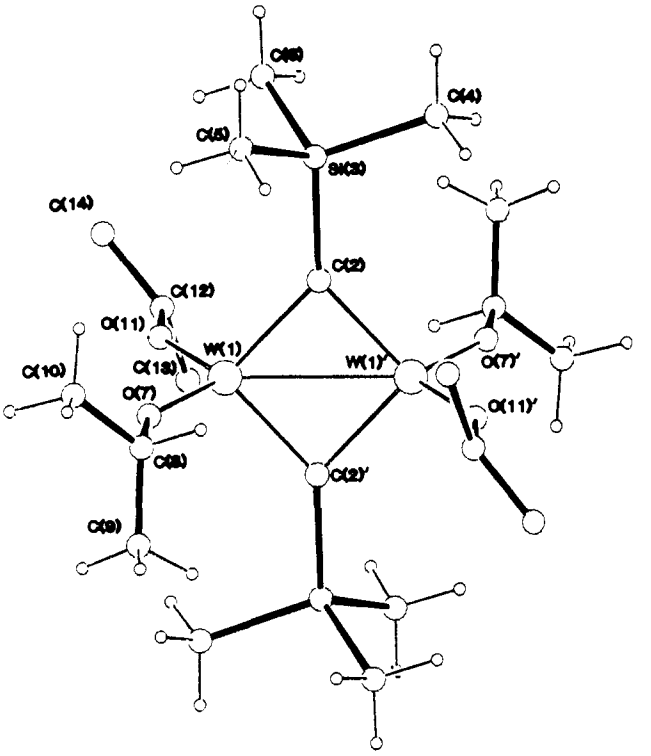

Figure 1. Ball-and-stick view of one of the $W_2(O\text{-}i\text{-}Pr)_4(\mu\text{-}CSiMe_3)_2$ molecules, **2**, showing the number scheme of the atoms. The other molecule found in the unit cell is virtually identical and is numbered similarly by using the following letter A; e.g., W(1) and W(1A) refer to tungsten atoms in molecules one and two, respectively.

alkyl vs. alkoxide. In this paper, we describe[9] our studies of the reactions between alkynes and $[X_2M(\mu\text{-}CSiMe_3)]_2$ compounds, where M = W and Ta and X = Me_3SiCH_2 and *i*-PrO. Pertinent to this study are the previous findings that the $W_2(\mu\text{-}C_2R_2)$-containing compounds, I, react with alkynes to give $W_2(\mu\text{-}C_4R_4)$ derivatives,[10] V, and of Cotton's discovery[11] of the formation of

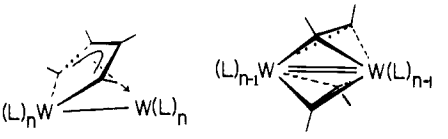

V VI

$[(t\text{-}BuO)_2W(\mu\text{-}CPh)]_2$ and $[(t\text{-}BuO)_2W(\mu\text{-}C_2Ph_2)]_2$ in the reaction between $W_2(O\text{-}t\text{-}Bu)_6$ and PhC≡CPh. The former compound is of type IV, while the latter has a central $W_2(\mu\text{-}C_2Ph_2)_2$ core shown in VI.

Results and Discussion

Starting Materials. The compound $W_2(CH_2SiMe_3)_4(\mu\text{-}CSiMe_3)_2$, **1**, and its tantalum analogue were prepared according to literature procedures.[4-6]

$W_2(O\text{-}i\text{-}Pr)_4(\mu\text{-}CSiMe_3)_2$, 2, was prepared by the addition of *i*-PrOH (ca. 6 equiv) to a hydrocarbon solution of **1**. Analogous reactions with EtOH proceed further to give the interesting tetranuclear compound $W_4(\mu\text{-}CSiMe_3)_2(OEt)_{14}$ by alcoholyses reactions involving both the alkyl and alkylidyne ligands.[12] Reactions involving *t*-BuOH proceed much more slowly, and a mixture of syn and anti isomers of $(t\text{-}BuO)(Me_3SiCH_2)W(\mu\text{-}$

(3) Hoffman, D. M.; Hoffman, R.; Fisel, C. R. *J. Am. Chem. Soc.* **1982**, *104*, 3858.
(4) Huq, F.; Mowat, W.; Skapski, A. C.; Wilkinson, G. *J. Chem. Soc., Chem. Commun.* **1971**, 1477.
(5) Anderson, R. A.; Gayler, A. L.; Wilkinson, G. *Angew. Chem., Int. Ed. Engl.* **1976**, *15*, 609.
(6) Chisholm, M. H.; Cotton, F. A.; Extine, M. W.; Murillo, C. A. *Inorg. Chem.* **1978**, *17*, 696.
(7) Bochmann, M.; Wilkinson, G.; Galas, A. M. R.; Hursthouse, M. B.; Abdul-Malik, K. M. *J. Chem. Soc., Dalton Trans.* **1980**, 1797.
(8) Chisholm, M. H.; Heppert, J. A., unpublished results.
(9) A preliminary report of one aspect of this work has appeared: Chisholm, M. H.; Heppert, J. A.; Huffman, J. C. *J. Am. Chem. Soc.* **1984**, *106*, 1151.
(10) Chisholm, M. H.; Hoffman, D. M.; Huffman, J. C. *J. Am. Chem. Soc.* **1984**, *106*, 6806.
(11) Cotton, F. A.; Schwotzer, W.; Shamshoum, E. S. *Organometallics* **1983**, *2*, 1167.
(12) Chisholm, M. H.; Heppert, J. A.; Huffman, J. C. *J. Am. Chem. Soc.*, submitted.

Table I. Fractional Coordinates and Isotropic Parameters for $W_2(O\text{-}i\text{-}Pr)_4(\mu\text{-}CSiMe_3)_2$

atom	10^4x	10^4y	10^4z	$10B_{iso}$
W(1)	5859 (1)	741 (1)	6044 (1)	36
C(2)	4967 (16)	668 (18)	3839 (20)	43
Si(3)	4977 (5)	1561 (6)	2401 (6)	51
C(4)	3877 (19)	858 (25)	519 (25)	73
C(5)	6260 (23)	1725 (30)	2537 (31)	87
C(6)	4809 (27)	3053 (27)	2644 (35)	90
O(7)	7216 (9)	555 (12)	6708 (15)	49
C(8)	7891 (19)	−90 (24)	6585 (35)	70
C(9)	8162 (38)	−920 (43)	7581 (63)	148
C(10)	8692 (36)	660 (42)	6555 (74)	183
O(11)	5796 (11)	2076 (11)	6927 (16)	50
C(12)	5175 (29)	2747 (27)	7128 (42)	94
C(13)	4754 (34)	2196 (40)	7897 (48)	127
C(14)	5457 (52)	3938 (58)	7145 (76)	88 (15)
C(14)*	4665 (54)	3413 (62)	6027 (79)	92 (16)
W(1A)	9282 (1)	4081 (1)	4796 (1)	37
C(2A)	9141 (12)	5405 (23)	3884 (22)	62
Si(3A)	8150 (5)	6264 (6)	2397 (7)	49
C(4A)	6789 (19)	5332 (24)	1578 (27)	67
C(5A)	8361 (26)	6599 (33)	862 (34)	96
C(6A)	8255 (24)	7724 (24)	3293 (35)	91
O(7A)	8606 (10)	3996 (14)	5826 (16)	55
C(8A)	8528 (32)	4617 (37)	6941 (41)	106
C(9A)	8533 (55)	3883 (42)	7933 (66)	189
C(10A)	7995 (38)	5511 (36)	6405 (46)	127
O(11A)	8885 (11)	2742 (12)	3487 (16)	53
C(12A)	8996 (29)	2127 (25)	2435 (36)	90
C(13A)	8927 (27)	927 (28)	2578 (36)	100
C(14A)	8296 (31)	2534 (32)	926 (33)	101

Table II. Selected Bond Distances for $W_2(\mu\text{-}CSiMe_3)_2(O\text{-}i\text{-}Pr)_4$ (Molecules 1 and 2)

A	B	distance, Å
	Molecule 1	
W(1)	W(1)′	2.622 (2)
W(1)	O(7)	1.86 (1)
W(1)	O(11)	1.84 (1)
W(1)′	C(2)	1.93 (2)
W(1)	C(2)	1.97 (2)
Si(3)	C(2)	1.86 (2)
O(7)	C(8)	1.43 (3)
O(11)	C(12)	1.42 (3)
Si(3)	C(Me)	1.84 (3) av
	Molecule 2	
W(1A)	W(1A)′	2.618 (2)
W(1A)	O(7A)	1.87 (1)
W(1A)	O(11A)	1.85 (1)
W(1A)′	C(2A)	1.80 (3)
W(1A)	C(2A)	2.00 (2)
Si(3A)	C(2A)	1.94 (2)
O(7A)	C(8A)	1.45 (3)
O(11A)	C(12A)	1.42 (3)
Si(3A)	C(Me)	1.87 (3) av

$CSiMe_3)_2W(CH_2SiMe_3)(O\text{-}t\text{-}Bu)$ is formed initially. These can be separated by fractional crystallization, but proof of structure by single crystal X-ray studies has not been sought. Only the isopropoxy compound **2** is used in this study.

Solid-State and Molecular Structure of 2. An ORTEP view of the $W_2(O\text{-}i\text{-}Pr)_4(\mu\text{-}CSiMe_3)_2$ molecule, **2**, is given in Figure 1. Atomic positional parameters are given in Table I. Listings of selected bond distances and bond angles are given in Tables II and III, respectively. There are two crystallographically independent molecules in the asymmetric unit, each lying at a crystallographic center. The two molecules are seen to be chemically equivalent and are isostructural with the starting material **1**. The W–W distance, 2.62 Å (averaged), is notably longer than that in **1** (2.53 Å) but similar to that reported by Cotton et al.[11] for $W_2(O\text{-}t\text{-}Bu)_4(\mu\text{-}CPh)_2$. The lengthening of the W–W bond which accompanies the replacement of Me_3SiCH_2 ligands by O-*i*-Pr ligands in going from **1** to **2** can reasonably be viewed as a consequence of RO-to-W π-bonding.[11] The short W–O distances

Table III. Selected Bond Angles for $W_2(\mu\text{-}CSiMe_3)_2(O\text{-}i\text{-}Pr)_4$ (Molecules 1 and 2)

A	B	C	angle, deg
	Molecule 1		
O(7)	W(1)	O(11)	115.1 (6)
O(7)	W(1)	C(2)	111.9 (7)
O(11)	W(1)	C(2)′	111.5 (7)
O(11)	W(1)	C(2)	110.0 (7)
O(11)	W(1)	C(2)′	111.2 (7)
C(2)	W(1)	C(2)′	95.6 (7)
W(1)	O(7)	C(8)	149.2 (14)
W(1)	O(11)	C(12)	148.6 (18)
W(1)	C(2)	W(1)′	84.4 (7)
W(1)	C(2)	Si(3)	136.2 (11)
W(1)′	C(2)	Si(3)	139.4 (11)
	Molecule 2		
O(7A)	W(1A)	O(11A)	114.6 (6)
O(7A)	W(1A)	C(2A)′	114.0 (8)
O(7A)	W(1A)	C(2A)	110.0 (8)
O(11A)	W(1A)	C(2A)′	111.2 (7)
O(11A)	W(1A)	C(2A)	111.9 (8)
C(2A)	W(1A)	C(2A)′	93.1 (8)
W(1A)	O(7A)	C(8A)	144.8 (20)
W(1A)	O(11A)	C(12A)	149.3 (17)
W(1A)	C(2A)	W(1A)′	86.9 (8)
W(1A)′	C(2A)	Si(3A)	127.7 (15)
W(1A)	C(2A)	Si(3A)	145.4 (15)

[1.85 Å (averaged)] in **2** are indicative of RO^- ligands acting as strong four-electron donors, $\sigma^2 + \pi^2$. The averaged W–C (alkylidyne) distances of 1.92 Å are similar to those observed in **1** and $W_2(O\text{-}t\text{-}Bu)_4(\mu\text{-}CPh)_2$. The central 1,3-$M_2C_2$ core of this molecule is comprised of a delocalized four-electron cyclobutadiene-like π system, and each W–C bond can, therefore, be considered to have a bond order of $1^1/_2$.

Reactions of 1 and 2 with Alkynes. General Considerations. We have restricted our studies to reactions involving ethyne and simple mono- and disubstituted acetylenes where the substituents were methyl, phenyl, and trimethylsilyl.

In hydrocarbon solvents, **1** reacts very rapidly at room temperature with ethyne and monosubstituted acetylenes to give products of insertion into one of the alkylidyne ligands. These reactions, when carried out at low temperatures and followed by NMR spectroscopy, are seen to proceed via initial formation of 1:1 alkyne adducts. Reactions employing MeC≡CMe and PhC≡CMe proceed more slowly at room temperature, and 1:1 alkyne adducts have been isolated and characterized. These do, however, react further, giving products of insertion into one of the μ-$CSiMe_3$ ligands. Reaction between **1** and PhC≡CPh is very sluggish at room temperature. Alkyne adduct formation is less favorable though evidence for a small concentration of an alkyne adduct is seen in ^1H NMR spectra of **1** in toluene-d_8 in the presence of a 10-fold excess of PhC≡CPh. At elevated temperatures, **1** and PhC≡CPh react to give a product of insertion similar to those of the other substituted alkyne.

2 and alkynes react similarly to give products of insertion into one of the μ-$CSiMe_3$ bonds. However, alkyne adducts appear less stable, and only in the reaction between **2** and $*C_2H_2$, where *C represents 92.5% ^{13}C, at low temperatures has a 1:1 alkyne adduct been seen.

We propose that the reactions between **1** or **2** and alkynes conform to a general scheme shown in eq I.

$$X_4W_2(\mu\text{-}CSiMe_3)_2 + R^1C{\equiv}CR^2 \xrightarrow{k_1} X_4W_2(\mu\text{-}CSiMe_3)_2(R^1CCR^2) \quad \text{(Ia)}$$

$$X_4W_2(\mu\text{-}CSiMe_3)_2(R^1CCR^2) \xrightarrow{k_2} X_4W_2(\mu\text{-}CSiMe_3)(\mu\text{-}CR^1CR^2CSiMe_3) \quad \text{(Ib)}$$

We have no evidence for the reverse step in reactions Ia and b. In general, when X = CH_2SiMe_3, steric factors influence k_1 and k_2 in a similar manner and $k_1 > k_2$ which allows the sequential observation of alkyne adduct and insertion product. The only

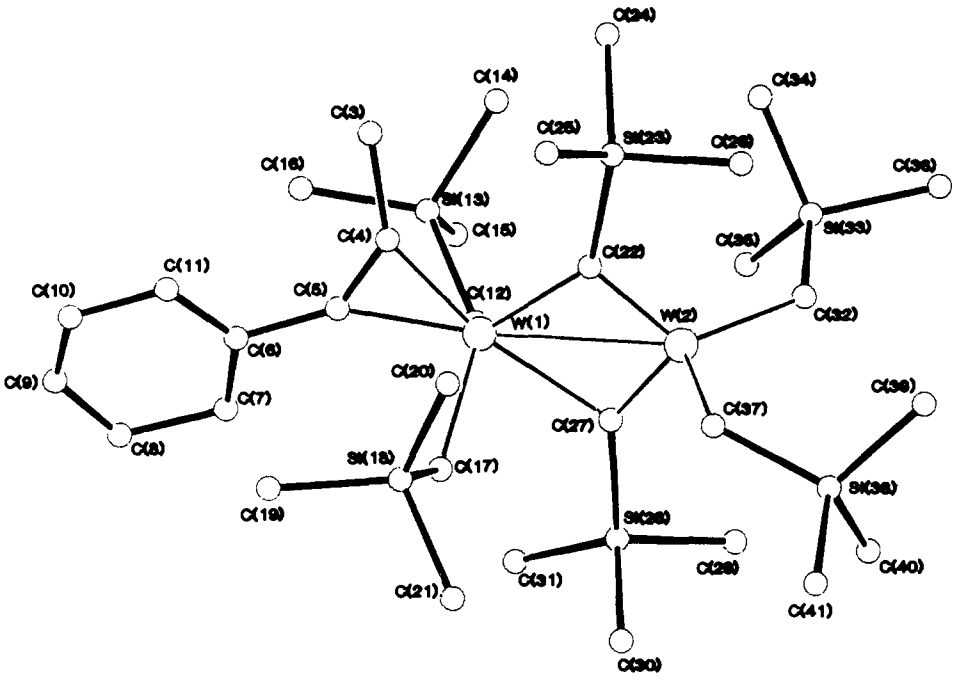

Figure 2. Ball-and-stick view of the $W_2(CH_2SiMe_3)_4(\mu\text{-}CSiMe_3)_2(\eta^2\text{-}PhC_2Me)$ molecule, **6b**, showing the number scheme for the atoms used in the tables.

exception to the latter involves the reaction between **1** and PhCCPh where alkyne adduct formation is so slow relative to the insertion reaction that the alkyne adduct is only detected when PhCCPh is present in greater than a 5-fold excess.

By contrast, the tantalum analogue does not react with ethyne, MeCCMe, or PhCCPh, even upon heating or photolysis in toluene solution. Polymerization of acetylenes, particularly ethyne, is observed in these and other reactions involving **1** and **2**. It is not known what is responsible for this polymerization, but it is not pertinent to the chemistry described above.

The new compounds are orange or brown waxy solids. They are air-sensitive and soluble, often extremely soluble in hydrocarbon solvents. This has led to problems in obtaining crystalline samples suitable for elemental analyses and single-crystal studies. However, NMR spectroscopy has proved a powerful and reliable means of analysis for noncrystalline samples. ^1H and ^{13}C NMR data for the insertion products, the 1,3-dimetallaallyl derivatives, are given in Tables IV and V, respectively. ^1H and ^{13}C NMR data for the 1:1 alkyne adducts are summarized in Table VI.

Since for a reaction involving **1** or **2** with an alkyne more than one product can sometimes be obtained, our assignment of a number followed by **a**, **b**, or **c** refers to the thermodynamic product of insertion as **a**, the 1:1 alkyne adduct as **b**, and the kinetically formed insertion product as **c**.

Alkyne Adducts. The only alkyne adducts which have been isolated in the solid state are the compounds $W_2(CH_2SiMe_3)_4(\mu\text{-}CSiMe_3)_2(R^1CCR^2)$, where $R^1 = R^2 = Me$ and $R^1 = Me$ and $R^2 = Ph$. Several others have been detected by NMR studies, and a self-consistent picture emerges starting with the one structurally characterized molecule.

Molecular Structure of $W_2(CH_2SiMe_3)_4(\mu\text{-}CSiMe_3)_2$(PhCCMe), 6b. A view of the molecule giving the atom number scheme is shown in Figure 2. This view is nearly perpendicular to the W-to-W axis and emphasizes the pseudo-trigonal-bipyramidal geometry about W(1) and the near tetrahedral geometry about W(2). In this description of the molecule, the η^2-alkyne ligand occupies an axial position of the trigonal bipyramid as does one of the μ-$CSiMe_3$ ligands. The two Me_3SiCH_2 ligands and the other μ-$CSiMe_3$ ligand occupy equatorial sites.

Figure 3 provides another view of molecule **6b** and shows the near planarity of the $(\eta^2\text{-}C_2)W_2(\mu\text{-}CSi)_2$ moiety.

Atomic positional parameters are given in Table VII and selected bond distances and angles are given in Tables VIII and IX, respectively. Though the quality of the structure is poor, it does

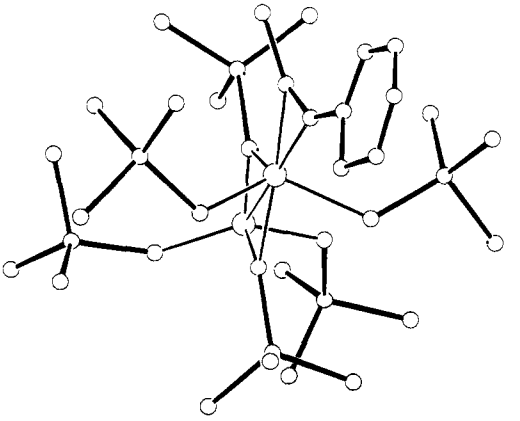

Figure 3. View of the $W_2(CH_2SiMe_3)_4(\mu\text{-}CSiMe_3)_2(\eta^2\text{-}PhC_2Me)$ molecule, **6b**, looking obliquely down the W–W axis, emphasizing the near planarity of the $W_2(\mu\text{-}CSi)_2(\eta^2\text{-}C_2)$ unit.

provide a sound foundation for the type of alkyne adduct involved in this study. (1) The alkyne is bonded to only one metal atom in a η^2 manner. (2) The W-to-W distance, 2.9 Å, represents a nonbonding distance, comparable to that in the d^0–d^0 dimer $(Me_3SiCH_2)_4Nb_2(\mu\text{-}CSiMe_3)_2$.[4] (3) As with several other early transition-metal η^2-alkyne adducts recently characterized, such as $[NbCl_3(PhCCPh)]_4$[14] and $(t\text{-}BuO)_4W(PhCCPh)$,[15] the η^2-alkyne can be viewed as a 2– ligand. (4) The gross asymmetry of the W–C distances within the central $W_2(\mu\text{-}CSiMe_3)_2$ unit is understood in terms of the valence bond description of the molecule shown in VII.

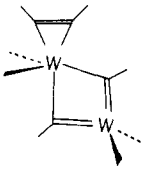

VII

(13) Chisholm, M. H. *Polyhedron* **1983**, *2*, 681.
(14) Hey, E.; Weller, F.; Dehnicke, K. *Naturwissenschaften* **1983**, *70*, 41.
(15) Theopold, K. H.; Holmes, S. J.; Schrock, R. R. *Angew. Chem., Int. Ed. Engl.* **1983**, *22*, 1010.

Table IV. ^{1}H NMR Spectral Data (360 MHz) for 1,3-Dimetallaallyl Insertion Products

compd (solvent, T °C)	R (1)	R (2)	R (3)	other
$W_2[\mu$-C(H)C($SiMe_3$)C(H)]-(μ-$CSiMe_3$)(CH_2SiMe_3)$_4$ (**3a**) (toluene-d_8, 20 °C)	C–H 5.87 (1 H, s, $^4J_{H_A-H_{A'}}$ = 11.5 Hz)	C–SiMe 0.2 (9 H, s)	C–H 5.87 (1 H, s, $J_{H_A-H_{A'}}$ = 11.5 Hz)	0.54 (9 H, s, μ-CSiMe_3) 0.20 (36 H, s, $CH_2Si$$Me_3$) 0.28, 0.05 (2 H, d, J_{A-X} = 11 Hz, CH_2SiMe_3)
$W_2[\mu$-C(H)C(H)C($SiMe_3$)]-(μ-$CSiMe_3$)(CH_2SiMe_3)$_4$ (**3c**) (toluene-d_8, −40 °C)	C–H 5.89 (1 H, br s)	C–H 9.26 (1 H, br s)	C–$SiMe_3$	
$W_2[\mu$-C(H)C(Me)C($SiMe_3$)]-(μ-$CSiMe_3$)(CH_2SiMe_3)$_4$ (**4a**) (toluene-d_8, 22 °C)	C–H 5.74 (1 H, s)	C–Me 2.18 (3 H, s)	C–$SiMe_3$ 0.33 (9 H, s)	0.52 (9 H, s, μ-CSiMe_3) 0.32 (18 H, s, $CH_2Si$$Me_3$) 0.20 (18 H, s, $CH_2Si$$Me_3$) 1.52, 0.36 (2 H, d, J_{A-X} = 10.8 Hz, CH_2SiMe_3) 1.11, 0.12 (2 H, d, J_{B-Y} = 1.8 Hz, CH_2SiMe_3)
$W_2[\mu$-C(Me)C(Me)C($SiMe_3$)]-(μ-$CSiMe_3$)(CH_2SiMe_3)$_4$ (**5a**) (toluene-d_8, −20 °C)	C–Me 2.58 (3 H, s)	C–Me 1.58 (3 H, s)	C–$SiMe_3$ 0.30 (9 H, s)	0.44 (9 H, s, μ-CSiMe_3) 0.37 (18 H, s, $CH_2Si$$Me_3$) 0.13 (18 H, s, $CH_2Si$$Me_3$) 3.03, 0.06 (2 H, d, J_{A-X} = 12 Hz, CH_2SiMe_3) 2.22, 0.36 (2 H, d, J_{B-Y} = 14 Hz, CH_2SiMe_3)
$W_2[\mu$-C(Me)C(Ph)C($SiMe_3$)]-(μ-$CSiMe_3$)(CH_2SiMe_3)$_4$ (**6a**) (toluene-d_8, −40 °C)	C–Me 2.46 (3 H, s)	C–Ph 7.0–6.7 (5 H, m)	C–$SiMe_3$ 0.20 (9 H, s)	0.65 (9 H, s, μ-CSiMe_3) 0.39 (18 H, s, $CH_2Si$$Me_3$) −0.08 (18 H, s, $CH_2Si$$Me_3$) 2.84, 0.01 (2 H, d, J_{A-X} = 13 Hz, CH_2SiMe_3) 1.64, 0.20 (2 H, d, J_{B-Y} = 14 Hz, CH_2SiMe_3)
$W_2[\mu$-C(Ph)C(Ph)C($SiMe_3$)]-(μ-$CSiMe_3$)(CH_2SiMe_3)$_4$ (**7a**) (toluene-d_8, 22 °C)	C–Ph 7.6 (2 H, m) 7.4 (1 H, m) 7.3 (2 H, m)	C–Ph 7.0 (2 H, m) 6.8 (1 H, m) 6.5 (2 H, m)	C–$SiMe_3$ 0.11 (9 H, s)	0.58 (9 H, s, μ-CSiMe_3) 0.36 (18 H, s, $CH_2Si$$Me_3$) 0.00 (18 H, s, $CH_2Si$$Me_3$) 2.19, 0.13 (2 H, d, J_{H_A-X} = 12 Hz, CH_2SiMe_3) 1.84, 0.28 (2 H, d, J_{H_B-Y} = 14 Hz, CH_2SiMe_3)
$W_2[\mu$-C(Ph)C(H)C($SiMe_3$)]-(μ-$CSiMe_3$)(CH_2SiMe_3)$_4$ (**8a**) (toluene-d_8, −40 °C)	C–Ph 7.13 (1 H, m) 7.02 (2 H, m) 6.74 (2 H, m)	C–H 9.57 (1 H, s)	C–$SiMe_3$ 0.14 (9 H, s)	0.51 (9 H, s, μ-CSiMe_3) 0.30 (18 H, s, $CH_2Si$$Me_3$) −0.14 (18 H, s, $CH_2Si$$Me_3$) 2.58, 0.06 (2 H, d, J_{A-X} = 13 Hz, CH_2SiMe_3) 1.52, 0.37 (2 H, d, J_{B-Y} = 13 Hz, CH_2SiMe_3)
$W_2[\mu$-C(H)C(Ph)C($SiMe_3$)]-(μ-$CSiMe_3$)(CH_2SiMe_3)$_4$ (**8c**)	C–H 6.09 (1 H, s)	C–Ph 7.51 (1 H, m) 7.08 (2 H, m) 7.00 (2 H, m)	C–$SiMe_3$ 0.17 (9 H, s)	0.49 (9 H, s, μ-CSiMe_3) 0.26 (18 H, s, $CH_2Si$$Me_3$) −0.14 (18 H, s, $CH_2Si$$Me_3$)
$W_2[\mu$-C(H)C($SiMe_3$)C(Ph)]-(μ-$CSiMe_3$)(CH_2SiMe_3)$_4$ (**8d**)	C–H 5.32 (1 H, s)	C–$SiMe_3$	C–Ph	
$W_2[\mu$-C(H)C($SiMe_3$)C($SiMe_3$)]-(μ-$CSiMe_3$)(CH_2SiMe_3)$_4$ (**9a**) (toluene-d_8, 35 °C)	C–H 6.62 (1 H, s)	C–$SiMe_3$ 0.34 (9 H, s)	C–$SiMe_3$ 0.15 (9 H, s)	0.56 (9 H, s, μ-CSiMe_3) 0.31 (18 H, s, $CH_2Si$$Me_3$) 0.14 (18 H, s, $CH_2Si$$Me_3$) 0.79, 0.06 (2 H, d, J_{A-X} = 11 Hz, CH_2SiMe_3) 0.42, 0.08 (2 H, d, J_{B-Y} = 14 Hz, CH_2SiMe_3)
$W_2[\mu$-C(H)C(H)C($SiMe_3$)]-(μ-$CSiMe_3$)(O-*i*-Pr)$_4$ (**10c**) (benzene-d_6, 22 °C)	C–H 5.41 (1 H, d, J_{H-H} = 3.6 Hz)	C–H 9.38 (1 H, d, J_{H-H} = 3.6 Hz, $J_{^{183}W-^1H}$ = 8.0 Hz)	C–$SiMe_3$ −0.10 (9 H, s)	0.51 (9 H, s, μ-CSiMe_3) 4.47 (2 H, dq, J_{Me-H} = 6.1 Hz, OCH(Me)$_2$) 4.06 (2 H, dq, J_{Me-H} = 6.1 Hz, OCH(Me)$_2$) 1.46, 1.25 (6 H, d, J_{Me-H} = 6.1 Hz, OCH(Me)$_2$) 1.21, 0.70 (6 H, d, J_{Me-H} = 6.1 Hz, OCH(Me)$_2$)

Table IV (Continued)

compd (solvent, T °C)	R (1)	R (2)	R (3)	other
	C–H	C–$SiMe_3$	C–H	
$W_2[\mu$-C(H)C($SiMe_3$)C(H)]-(μ-C$SiMe_3$)(O-*i*-Pr)$_4$ (**10a**) (benzene-d_6, 22 °C)	4.58 (1 H, s, $J_{H_A-H_{A'}}$ = 11 Hz)	0.43 (9 H, s)	4.58 (1 H, s, $J_{H_A-H_{A'}}$ = 11 Hz)	0.60 (9 H, s, μ-CSi*Me*$_3$) 0.41 (4 H, dq, J_{Me-H} = 6.1 Hz, OC*H*(Me)$_2$) 1.24, 0.81 (24 H, d, J_{Me-H} = 6.1 Hz, OCH(*Me*)$_2$)
	C–$SiMe_3$	C–H	C–$SiMe_3$	
$W_2[\mu$-C($SiMe_3$)C(H)C($SiMe_3$)]-(μ-C$SeMe_3$)(O-*i*-Pr)$_4$ (**11c**) (toluene-d_8, −25 °C)	0.03 (9 H, s)	9.78 (1 H, s, $J_{^{183}W-H}$ = 8.3 Hz)	0.03 (9 H, s)	0.60 (9 H, s, μ-CSi*Me*$_3$) 0.47 (4 H, dq, J_{Me-H} = 6.1 Hz, OC*H*(Me)$_2$) 1.37, 1.25 (24 H, d, J_{Me-H} = 6.1 Hz, OCH(*Me*)$_2$)
	C–H	C–$SiMe_3$	C–$SiMe_3$	
$W_2[\mu$-C(H)C($SiMe_3$)C($SiMe_3$)]-(μ-C$SiMe_3$)(O-*i*-Pr)$_4$ (**11a**) (toluene-d_8, 35 °C)	6.26 (1 H, s)	0.54 (9 H, s)	−0.02 (9 H, s)	0.62 (9 H, s μ-CSi*Me*$_3$) 4.73 (2 H, dq, J_{Me-H} = 6.1 Hz, OC*H*(Me)$_2$) 4.27 (2 H, dq, J_{Me-H} = 6.1 Hz, OC*H*(Me)$_2$) 1.54, 1.38 (6 H, d, J_{Me-H} = 6.1 Hz, OCH(*Me*)$_2$) 1.24, 0.75 (6 H, d, J_{Me-H} = 6.1 Hz, OCH(*Me*)$_2$)

In a formal sense, the addition of the alkyne to **1** may be viewed as an oxidative addition reaction. The two electrons in the M–M bond in **1** are used to back-bond to the alkyne. Just as the d^2 metal centers $NbCl_3$ and W(O-*t*-Bu)$_4$ are formally oxidized to d^0 in their formation of alkyne adducts, so too can the alkyne adduct **6b** be viewed as a W(6+)–W(6+), d^0–d^0 dimer. In this regard, it is worth noting that the tantalum analogue of **1**, being a d^0–d^0 dimer, does not form stable (detectable) alkyne adducts similar to **6b**.

Though the valence bond description shown in VII is simplistically appealing, it leaves a number of questions pertaining to the nature of the W_2–η^2-PhCCMe interaction unaddressed. A qualitative MO bonding description is also desirable.

Qualitative MO Description of the Bonding in 6b. The bonding at W(2) may be viewed quite straightforwardly as a W(6+) analogue of (*t*-BuO)$_2$MoO$_2$,[16] i.e., a pseudotetrahedral unit having two double bonds and two single bonds to carbon.

The bonding at W(1) can be considered to be derived from the bonding in trigonal-bipyramidal molecules.[17] As a point of origin, we can start with a ML_4 d^2 unit lacking an axial coordination site. This corresponds to the orbital picture shown on the left-hand side of Figure 4. L represents Me_3SiCH_2 and L′ the μ-C$SiMe_3$ ligands, all of which form essentially σ bonds to W(1). In the symmetry group C_s, there are two low-lying metal d orbitals, the d_{xz} and d_{yz}, taking the axial ligands to be coincident with the z axis. These are equivalent to the e″ orbitals in ML_5 molecules of D_{3h} symmetry and are not involved in M–L σ bonding. Above them in energy are two hybrid orbitals which are primarily d in character, remnants of the ($d_{x^2-y^2}$, d_{xy}) e′ set in ML_5 molecules of D_{3h} symmetry. Finally, there is a high-lying σ orbital, a d_{z^2}–p_z hybrid, which has been somewhat stabilized by the removal of the ligand, in forming our ML_4 fragment. This is a d^2 center because W(2) has been robbed of its share of the M–M bonding pair of electrons in forming the asymmetric alkylidyne bridges.

On the right in Figure 4, we show the now well-recognized representations for the π and π^* orbitals of a bent alkyne ligand.[18]

Allowing these two fragments to interact produces the qualitative MO scheme shown in the center of Figure 4. The essential feature of this diagram is the presence of three low-lying orbitals capable of accommodating six electrons, four from the alkyne and two from W(1). One interaction is of pure σ character involving the a′ filled orbital of the alkyne and the vacant a′ orbital on the metal, the d_{z^2}–p_z hybrid. The other two bonding interactions are of π character, one involving the filled π-bonding orbital of the acetylene and the other the antibonding LUMO of the bent alkyne fragment. Viewed in this way, the alkyne acts as both a π-donor and a π-acceptor ligand.

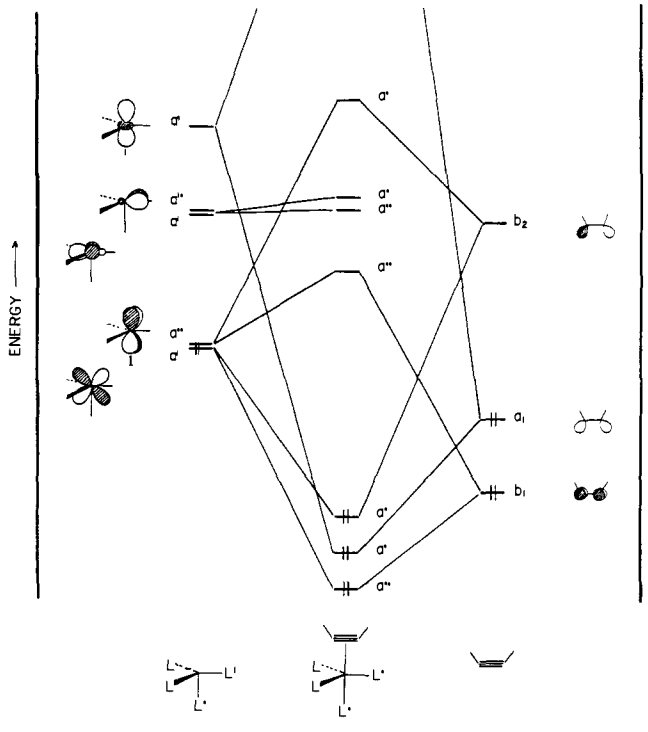

Figure 4. Qualitative MO diagram for the bonding of the alkyne to the trigonal-bipyramidal tungsten d^2 center in molecule **6b**. The frontier orbitals of the ML_4 and bent alkyne fragments are shown to the left and right, respectively, and their origin is discussed in the text.

This bonding description also suggests that there should be a relatively low barrier to rotation about the alkyne–metal vector since the idealized ML_4 fragment of a ML_5 (D_{3h}) molecule would have degenerate d_{xz} and d_{yz} orbitals. It seems likely that the d_{xz} and d_{yz} orbitals are still of similar energy in the present case.

This qualitative MO description also allows one to anticipate the effect of substituting a purely σ-donating ligand L, CH_2SiMe_3, by a σ- and π-donating *i*-PrO ligand. The filled p orbitals on the oxygen atoms will compete with the alkyne for interaction with the d_{xz}, d_{yz} orbitals, as well as interacting with the other vacant e set ($d_{x^2-y^2}$, d_{xy}). The net result of this competition will be the raising of the relative energies of the d_{xz} and d_{yz} orbital energies, thereby weakening the alkyne-to-metal bonding interaction.

(16) Chisholm, M. H.; Folting, K.; Huffman, J. C.; Kirkpatrick, C. C.; Ratermann, A. L. *J. Am. Chem. Soc.* **1981**, *103*, 1305.
(17) Rossi, A. R.; Hoffman, R. *Inorg. Chem.* **1975**, *14*, 365.
(18) Qualitative assignments of the shape and relative energy of the bent-alkyne frontier orbitals were taken from ref 3.

Table V. ^{13}C NMR Spectral Data (90.8 MHz) for 1,3-Dimetallaallyl Insertion Products

compound	C(1)	C(2)	C(3)	other
	C–H[1]	C–SiMe$_3$	C–H[1]	
3a	152.7 ($^1J_{^{13}C-^1H}$ = 161 Hz, $^3J_{^{13}C-^1H}$ = 13.5 Hz, $^2J_{^{13}C-^{13}C}$ = 11.5 Hz, $J_{^{183}W-^{13}C}$ = 32 Hz)	156.0	152.7	329.9 (μ-*C*SiMe$_3$, $J_{^{183}W-^{13}C}$ = 111 Hz) 76.0 (*C*H$_2$SiMe$_3$) 3.0 (CH$_2$Si*Me*$_3$) 2.4, −0.5 (CSi*Me*$_3$)
	C–H[1]	C–H[1]	C–SiMe$_3$	
3c	153.3 ($^1J_{^{13}C-^1H}$ = 160 Hz, $^1J_{^{13}C-^{13}C}$ = 31 Hz)	135.8 ($^1J_{^{13}C-^1H}$ = 159 Hz, $^1J_{^{13}C-^{13}C}$ = 31 Hz)		
	C–H	C–Me	C–SiMe$_3$	
4a	148.5 ($J_{^{183}W-^{13}C}$ = 28 Hz, $^1J_{^{13}C-^1H}$ = 154 Hz)	156.4	147.7 ($J_{^{183}W-^{13}C}$ = 30.7 Hz)	336.7 (μ-*C*SiMe$_3$, $J_{^{183}W-^{13}C}$ = 116.5 Hz) 80.3, 68.4 (*C*H$_2$SiMe$_3$, $J_{^{183}W-^{13}C}$ = 57, 72 Hz) 28.7 (*Me*-C) 3.3 (CH$_2$Si*Me*$_3$) 3.1 & 2.7 (CSi*Me*$_3$)
	C–Me	C–Me	C–SiMe$_3$	
5a	161.3 ($J_{^{183}W-^{13}C}$ = 24 Hz)	156.3	143.7 ($J_{^{183}W-^{13}C}$ = 30 Hz)	334.6 (μ-*C*SiMe$_3$, $J_{^{183}W-^{13}C}$ = 119 Hz) 76.1, 70.4 (*C*H$_2$SiMe$_3$) 24.5, 22.8 (*Me*-C) 3.3, 2.7 (CH$_2$Si*Me*$_3$) 2.3, 1.3 (CSi*Me*$_3$)
	C–Me	C–Ph	C–SiMe$_3$	
6a	166.7 ($J_{^{183}W-^{13}C}$ = 26 Hz)	145.4	144.7 ($J_{^{183}W-^{13}C}$ = 34 Hz)	341.3 (μ-*C*SiMe$_3$, $J_{^{183}W-^{13}C}$ = 113 Hz) 143.8, 137.9, 138.5, 127.1 (C–*Ph*) 86.6, 72.0 (*C*H$_2$SiMe$_3$, $J_{^{183}W-^{13}C}$ = 64, 74 Hz) 23.9 (C-*Me*) 3.4, 2.2 (CH$_2$Si*Me*$_3$) 3.9, 3.3 (CSi*Me*$_3$)
	C–Ph	C–Ph	C–SiMe$_3$	
7a	158.8	158.4	149.9	340.0 (μ-*C*SiMe$_3$, $J_{^{183}W-^{13}C}$ = 114 Hz) 144.0 (C-*Ph*, partial) 144.3 (C-*Ph*, partial) 90.3, 73.9 (*C*H$_2$SiMe$_3$, $J_{^{183}W-^{13}C}$ = 64, 73 Hz) 3.4, 2.2 (CH$_2$Si*Me*$_3$) 3.6, 3.2 (CSi*Me*$_3$)
	C–Ph	C–H	C–SiMe$_3$	340.0 (μ-*C*SiMe$_3$)
8a	170.8	137.1	146.2	142.6, 137.8, 135.8 (C-*Ph* partial) 84.9, 73.3 (*C*H$_2$SiMe$_3$) 2.8, 3.7 (CH$_2$Si*Me*$_3$) 4.0, 1.4 (C-Si*Me*$_3$)
	C–H	C–SiMe$_3$	C–SiMe$_3$	
9a	170.9 ($J_{^{13}C-^1H}$ = 154 Hz)	165.2	152.6	346.1 (μ-*C*SiMe$_3$) 83.5, 70.3 (*C*H$_2$SiMe$_3$, $J_{^{183}W-^{13}C}$ = 54, 76 Hz) 3.5, 3.4 (CH$_2$Si*Me*$_3$) 1.4, 2.8, 3.0 (C-Si*Me*$_3$)
	C–H[1]	C–H[1]	C–SiMe$_3$	
10c	179.2 ($J_{^{183}W-^{13}C}$ = 32 Hz, $^1J_{^{13}C-^{13}C}$ = 32 Hz)	113.5 ($^1J_{^{13}C-^{13}C}$ = 32 Hz, $^1J_{^{13}C-^1H}$ = 163 Hz)	150.0	320.7 (μ-*C*SiMe$_3$, $J_{^{183}W-^{13}C}$ = 114 Hz) 77.0, 75.7 (OCH(Me)$_2$) 26.7, 26.4, 25.7, 25.5 (OCH(*Me*)$_2$) 2.1, 1.6 (C-Si*Me*$_3$)
	C–H[1]	C–SiMe$_3$	C–H[1]	
10a	156.2 ($J_{^{183}W-^{13}C}$ = 37 Hz, $^1J_{^{13}C-^1H}$ = 151 Hz, $^2J_{^{13}C-^{13}C}$ = 11.2 Hz, $^3J_{^{13}C-^1H}$ = 12.5 Hz)	144.8	156.2	310.1 (μ-*C*SiMe$_3$) 76.9 (OCH(Me)$_2$) 26.1, 25.8 (OCH(*Me*)$_2$) 3.1, 2.2 (CSi*Me*$_3$)

NMR Studies of Alkyne Adducts. ^1H and ^{13}C NMR data for the alkyne adducts are given in Table VI.

η^2-Alkyne Group. The ^{13}C signal for the labeled ethyne ligand in **3b**, $W_2(CH_2SiMe_3)_4(\mu\text{-}CSiMe_3)_2(\eta^2\text{-}{}^*C_2H_2)$, where *C represents 92.5% atom ^{13}C, is shown in Figure 5. Even at −80 °C, only one ^{13}C signal is seen which implies that rotation about the alkyne–W vector is very rapid. The alternate explanation that the η^2-C_2H_2 ligand is bonded in a crosswise manner, that is, at right angles to that seen in **6b**, cannot be ruled out in this instance. However, as we shall show, the spectra obtained for the RCCH and PhCCMe adducts preclude this situation. The chemical shift of the ethyne carbons in **3b** is extremely deshielded and in a range seen for alkyne carbon atoms where the alkyne is acting as a four-electron donor.[19] The ^1H-coupled spectrum is also shown in Figure 5. This is part of an AA′ XX′ spectrum.

The ^{13}C NMR spectra recorded for the labeled compound $W_2(O\text{-}i\text{-}Pr)_4(\mu\text{-}CSiMe_3)_2(^*C_2H_2)$ in toluene-d_8 at low temperatures are qualitatively similar to those described above for **3b** and shown in Figure 5. Of note, however, is that the change from Me_3SiCH_2 to *i*-PrO in supporting ligands is accompanied by an upfield shift of ca. 30 ppm, a decrease in the magnitude of $J_{^{183}W-^{13}C}$, from 33 to 26 Hz, and an increase in the magnitude of $J_{^{13}C-^{13}C}$, 42–49 Hz.[20] All these changes are consistent with a weaker alkyne-to-tungsten interaction in the isopropoxy compound. The ^{13}C parameters for the $^*C_2H_2$ ligand in the isopropoxy compound are similar to those observed in $W_2(O\text{-}i\text{-}Pr)_6(\mu\text{-}C_4H_4)(\eta^2\text{-}{}^*C_2H_2)$ discussed previously.[21]

The ^1H NMR spectra of the 1:1 adducts of **1** with MeCCH, PhCCH, Me_3SiCCH, and PhCCMe show that an apparent mo-

(19) Templeton, J. L.; Ward, B. C. *J. Am. Chem. Soc.* **1980**, *102*, 3288.

(20) For a comparison, we note $^1J_{^{13}C-^{13}C}$ = 35, 68 and 172 Hz in ethane, ethylene, and ethyne, respectively. Smaller values of $J_{^{13}C-^{13}C}$ ca. 12 Hz are observed in three-membered organic rings: Marshall, J. L. *Meth. Stereochem. Anal.* **1983**, *2*, 1.

(21) $\delta(\eta^2\text{-}{}^{13}C_2H_2)$ = 179.3 ppm, $J_{^{183}W-^{13}C}$ = 40, $J_{^{13}C-^{13}C}$ = 54.5, $^1J_{^{13}C-H}$ = 198.2 Hz; Chisholm, M. H.; Hoffman, D. M.; Huffman, J. C. *J. Am. Chem. Soc.* **1984**, *106*, 6806.

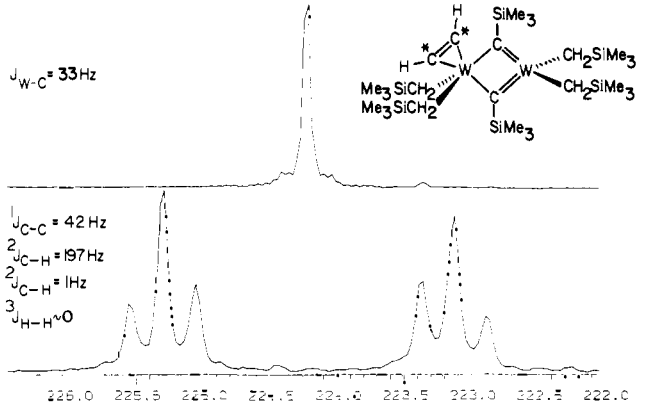

Figure 5. ^{13}C NMR spectra of the acetylenic carbon resonances in the labeled compound $W_2(CH_2SiMe_3)_4(\mu\text{-}CSiMe_3)_2(\eta^2\text{-}{}^*C_2H_2)$, where *C represents 92.5 atom % ^{13}C, recorded in toluene-d_8 at −40 °C, 90.8 MHz. The proton decoupled spectrum at the top reveals one time-averaged carbon signal for the η^2-C_2 moiety with coupling to ^{183}W, $I = {}^1/_2$, 14.5% natural abundance. The spectrum below shows the proton-coupled ^{13}C signals for the η^2-$^*C_2H_2$ moiety as the AA′ portion of the expected AA′XX′ spin system.[21] The relative signs of $^1J_{C-H}$ and $^2J_{C-H}$ are necessarily opposite and the relative signs of $^1J_{C-C}$ and $^3J_{H-H}$ remain undetermined.

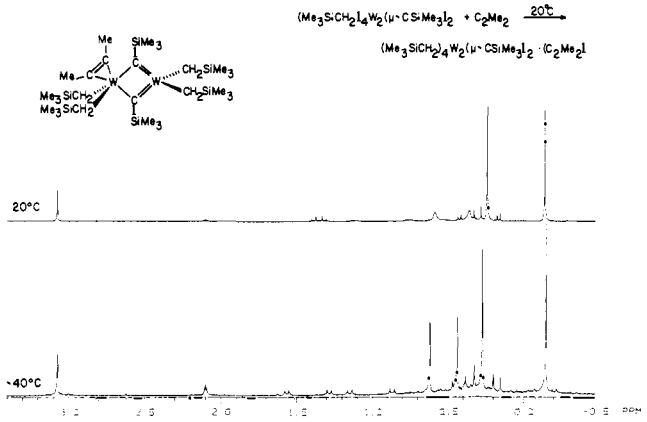

Figure 6. ^1H NMR spectrum of $W_2(CH_2SiMe_3)_4(\mu\text{-}CSiMe_3)_2(\eta^2\text{-}C_2Me_2)$, **5b**, recorded in toluene-d_8, 360 MHz, at +20 °C (top) and −40 °C (bottom) showing the stereochemically nonrigid nature of the molecule as described in the text.

lecular plane of symmetry exists in solution. This is consistent with the observed solid-state structure of **6b**. The spectra of the MeCCMe adduct is similar in this regard but only shows one alkyne methyl signal even at low temperatures. Thus, while we cannot be sure that all alkyne ligands bond in the ground state with their C–C vector aligned in the manner shown in Figure 3 for molecule **6b**, the NMR data are most readily interpretable in terms of facile rotation about the alkyne–tungsten vector.

The ^1H NMR signals of the Me_3SiCH_2 and Me_3SiC ligands are also informative. At low temperatures, there are two types of Me_3SiCH_2 ligands in the integral ratio 2:2 each with diastereotopic methylene protons. The Me_3SiC proton signals appear as two singlets in the ratio 1:1. Many of the compounds are only stable at low temperatures, and these spectra are sufficient to characterize the alkyne adduct as one of the type found for **6b**. However, in the case of the alkyne adducts involving MeCCMe and PhCCMe, insertion into a μ-$CSiMe_3$ ligand is sufficiently slow that a fluxional process can be observed at ambient temperatures.

The spectra recorded at −40 and +20 °C for the dimethylacetylene adduct **5b** in toluene-d_8 are shown in Figure 6.

When the temperature is raised, one of the AB quartet resonances centered around 1 ppm becomes broad and the two signals corresponding to the μ-$CSiMe_3$ ligands at 0.61 and 0.43 ppm go into the base line. These changes do not affect the signals of the η^2-C_2Me_2 ligand nor the methyl signals of the CH_2SiMe_3 groups. Evidently the fluxional process does not involve the alkyne ligand migrating between the two tungsten atoms.

Scheme I. Representations of Two Possible Fluxional Processes for the Alkyne Adduct 5b[a]

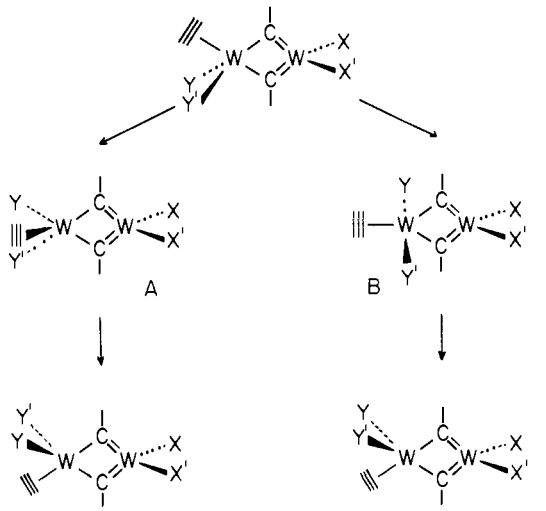

[a] Path A represents a rotation of the Y, Y′, and alkyne ligands about the W–W axis, while path B represents an inversion of the Y, Y′, and alkyne ligands at the tungsten center. As discussed in the text, the ^1H NMR data preclude path B.

We believe the most plausible interpretation of the NMR data involves a pseudorotation of the ligands at the five-coordinate tungsten center as shown in Scheme I. This pseudorotation (see A in Scheme I) causes the μ-$CSiMe_3$ groups to become equivalent, and by generating an additional plane of symmetry in the molecule, the methylene protons of the CH_2SiMe_3 ligands attached to W(2) (X and X′ in Scheme I) become equivalent. The methylene protons of the CH_2SiMe_3 ligands attached to W(1), those ligands which are involved in the pseudorotation process, remain diastereotopic. An inversion pathway (see B in Scheme I) can be ruled out as both pairs of methylene protons would loose their diastereotopic character.

Insertion Products: 1,3-Dimetallaallyl Derivatives. Two compounds have been structurally characterized, namely **7a**, the insertion product obtained in the reaction between PhCCPh and **1**, and **10c**, the kinetically favored insertion product formed in the reaction between **2** and HCCH.

Molecular Structures of $(Me_3SiCH_2)_4W_2(\mu\text{-}CSiMe_3)(\mu\text{-}C(Ph)C(Ph)CSiMe_3)$, 7a, and $(i\text{-}PrO)_4W_2(\mu\text{-}CSiMe_3)(\mu\text{-}CHCHCSiMe_3)$, 10c. ORTEP views of the two molecules, **7a** and **10c**, giving the atom number scheme are shown in Figures 7 and 8, respectively. Atomic positional parameters are given in Tables X (**7a**) and XI (**10c**). Selected bond distances are given in Tables XII (**7a**) and XIII (**10c**) and bond angles in Tables XIV (**7a**) and XV (**10c**).

The salient features of the structures are as follows. (1) In both molecules, the W–W distances are in the range observed for W–W single bonds in the presence of bridging ligands.[22] The W-to-W distance in **10c** is notably longer than that in **7a** but by a similar magnitude as that seen for the W–W distances in **1** and **2**. (2) The four α carbon atoms of the Me_3SiCH_2 ligands and the two tungsten atoms in **7a** lie roughly in a plane as do the four oxygen atoms and the two tungsten atoms in **10c**. (3) In each molecule, the W–C distances to the μ-$CSiMe_3$ ligand are essentially identical. (4) The μ-$CPhCPhCSiMe_3$ ligand in **7a** and the μ-$CHCHCSiMe_3$ ligand in **10c** are not symmetrically bonded to the two tungsten atoms. This is most evident from a consideration of the W to C-2 or β carbons of the allyl ligand. In the case of molecule **7a**, the distortion from a symmetrically bridged $CPhCPhCSiMe_3$ ligand

(22) See, for example, W–W distances in $W_2(O\text{-}i\text{-}Pr)_6(\mu\text{-}X)$ compounds where X = C_2R_2, C_4R_4, CHCHCRN, and $CH_2CHC(R)CN$: ref 1, 10, and: Chisholm, M. H.; Hoffman, D. M.; Huffman, J. C. *J. Am. Chem. Soc.* **1984**, *106*, 6815.

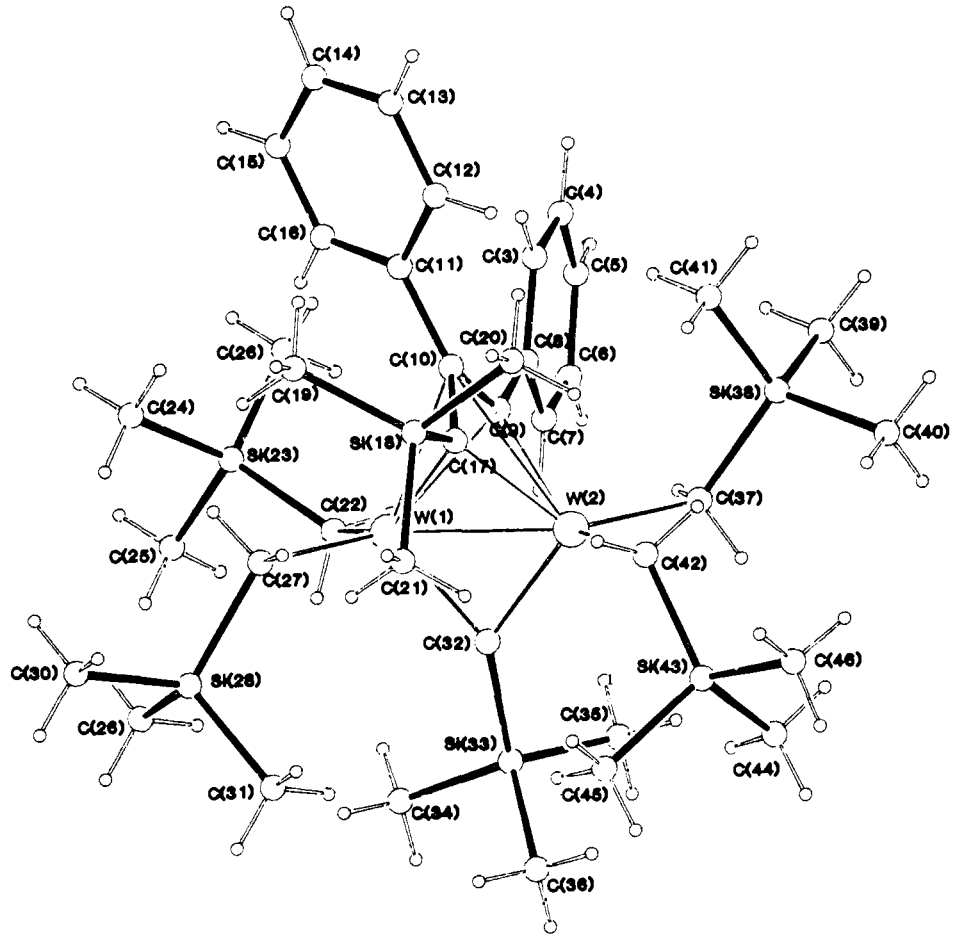

Figure 7. Ball-and-stick view of the $W_2(CH_2SiMe_3)_4(\mu\text{-}CSiMe_3)(\mu\text{-}CPhCPhCSiMe_3)$ molecule, **7a**, giving the atom number scheme used in the table.

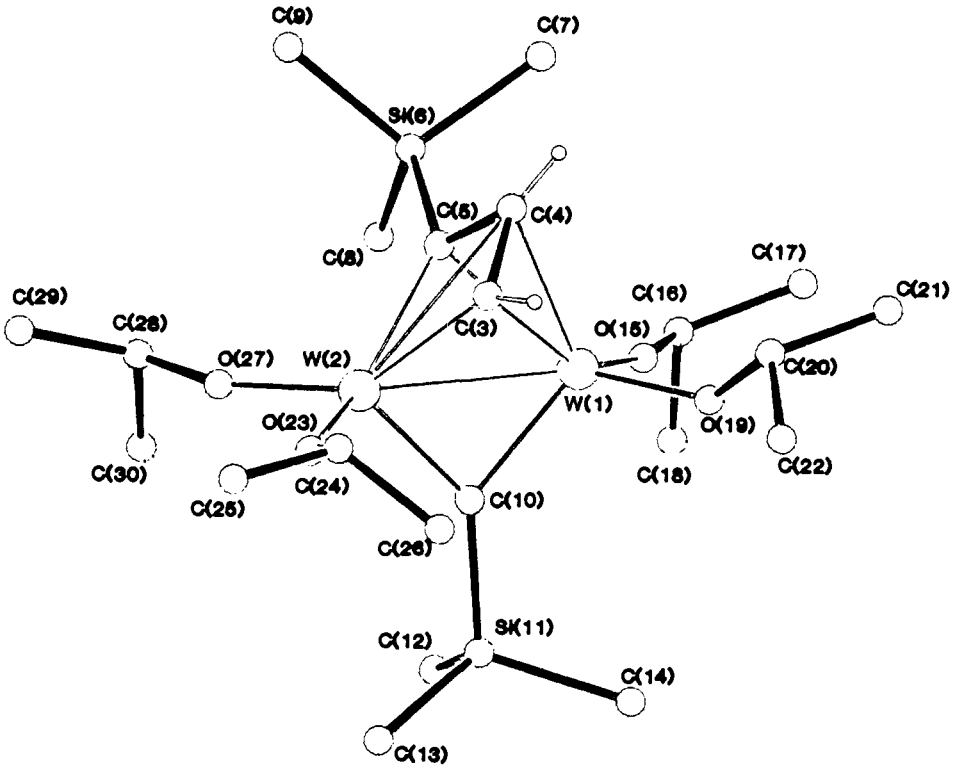

Figure 8. Ball-and-stick view of the $W_2(O\text{-}i\text{-}Pr)_4(\mu\text{-}CSiMe_3)(\mu\text{-}CHCHCSiMe_3)$ molecule, **10c**, giving the atom number scheme used in the tables.

might be viewed to result from intra- or even intermolecular steric forces. However, the distortion in **10c** is even more pronounced, and here the hydrogen atom substituent on the β carbon minimizes steric repulsions at that position. In **10c**, W(2) and the three carbon atoms of the allyl ligand are in a plane, and W(1) may be considered to be η^4-bonded to a tungstacyclobutadiene. (5) Within both molecules, certain abnormalities of bond distances and bond angles can be traced to the effects of internal steric

Table VI. ^1H and ^{13}C NMR Spectral Data for Alkyne Monoadducts

compound	^1H NMR spectral data (δ)	^{13}C NMR spectral data (δ)
$W_2(\mu\text{-}CSiMe_3)_2(CH_2SiMe_3)_4\cdot(C_2H_2)$ (**3b**) (toluene-d_8, −70 °C)	12.9 (2 H, s, C_2H_2) 0.68, 0.60 (9 H, s, C-SiMe_3) 0.18, −0.26 (18 H, s, CH_2SiMe_3)	216.8 ($^{13}C_2H_2$, $J_{^{183}W-^{13}C}$ = 33, $^1J_{^{13}C-^{13}C}$ = 42, $^1J_{^{13}C-^1H}$ = 197, $^2J_{^{13}C-^1H}$ = 1 Hz)
$W_2(\mu\text{-}CSiMe_3)_2(CH_2SiMe_3)_4\cdot[C_2(H)(Me)]$ (**4b**) (toluene-d_8, −70 °C)	12.3 (1 H, s, $C_2(H)$(Me)) 3.50 (3 H, s, C_2(H)(Me)) 0.69, 0.62 (9 H, s, C-SiMe_3) 0.23, −0.32 (18 H, s, CH_2SiMe_3)	
$W_2(\mu\text{-}CSiMe_3)_2(CH_2SiMe_3)_4\cdot[C_2(Me)_2]$ (**5b**) (toluene-d_8, −70 °C)	3.06 (6 H, s, C_2Me_2) 0.61, 0.43 (9 H, s, C-SiMe_3) 0.26, −0.15 (18 H, s, CH_2SiMe_3) 1.55, 1.27 (2 H, d, $J_{H_A-H_{A'}}$ = 10 Hz, CH_2SiMe_3) 1.13, 0.85 (2 H, d, $J_{H_B-H_{B'}}$ = 11 Hz, CH_2SiMe_3)	359.0, 339.4 (μ-CSiMe$_3$, $J_{^{183}W-^{13}C}$ = 121, 80 Hz) 221.0 (C_2Me_2) 66.1, 64.8 (CH_2SiMe_3, $J_{^{183}W-^{13}C}$ = 80, 106 Hz) 22.5 (C_2Me_2) 2.9 (CH_2SiMe_3) 4.3, 3.3 (μ-CSiMe_3)
$W_2(\mu\text{-}CSiMe_3)_2(CH_2SiMe_3)_4\cdot[C_2(Me)(Ph)]$ (**6b**) (toluene-d_8, 22 °C)	7.97, 7.34, 7.16 (5 H, M, C_2(Me)(Ph)) 3.38 (3 H, s, C_2(Me)(Ph)) 0.62, 0.35 (9 H, s, C-SiMe_3) 0.26, −0.29 (18 H, s, CH_2SiMe_3) 1.87, 1.34 (2 H, d, $J_{H_A-H_{A'}}$ = 10 Hz, CH_2SiMe_3) 1.12, 0.80 (2 H, d, $J_{H_B-H_{B'}}$ = 10 Hz, CH_2SiMe_3)	359.7, 339.0 (μ-CSiMe$_3$) 223.9, 210.1 (C_2(Me)(Ph)) 139.5, 133.6, 130.9, 129.7 (C_2(Me)(Ph)) 66.6, 65.8 (CH_2SiMe_3) 25.5 (C_2(Me)(Ph)) 3.4 (CH_2SiMe_3) 4.8, 3.4 (μ-CSiMe_3)
$W_2(\mu\text{-}CSiMe_3)_2(CH_2SiMe_3)_4\cdot[C_2(H)(Ph)]$ (**8b**) (toluene-d_8, −40 °C)	13.09 (1 H, s, $C_2(H)$(Ph)) 8.1, 7.4, 7.2 (5 H, m, C_2(H)(Ph)) 0.82, 0.75 (9 H, s, C-SiMe_3) 0.26, 0.48 (18 H, s, CH_2SiMe_3) 2.85, 0.68 (2 H, d, $J_{H_A-H_{A'}}$ = 10 Hz, CH_2SiMe_3) 1.09, 0.90 (2 H, d, $J_{H_A-H_{A'}}$ = 10 Hz, CH_2SiMe_3)	
$W_2(\mu\text{-}CSiMe_3)_2(CH_2SiMe_3)_4\cdot[C_2Ph_2]$ (**7b**) (toluene-d_8, 23 °C, partial)	0.61, 1.07 (9 H, s, C-SiMe_3) 0.30, −0.17 (18 H, s, CH_2SiMe_3) 2.32, 0.71 (2 H, d, $J_{H_A-H_{A'}}$ = 9.7 Hz, CH_2SiMe_3) 1.32, 1.07 (2 H, d, $J_{H_A-H_{A'}}$ = 9.7 Hz, CH_2SiMe_3)	
$W_2(\mu\text{-}CSiMe_3)_2(CH_2SiMe_3)_4\cdot[C_2(H)(SiMe_3)]$ (**9b**) (toluene-d_8, −40 °C)	13.54 (1 H, s, $C_2(H)$(SiMe_3)) 0.65, 0.62 (9 H, s, CSiMe_3) 0.60 (9 H, s, C_2(H)(SiMe_3)) 0.32, −0.36 (18 H, s, CH_2SiMe_3) 2.28, 0.57 (2 H, d, $J_{H_A-H_{A'}}$ = 9 Hz, CH_2SiMe_3) 0.99, 0.89 (2 H, d, $J_{H_B-H_{B'}}$ = 12 Hz, CH_2SiMe_3)	
$W_2(\mu\text{-}CSiMe_3)_2(O\text{-}i\text{-}Pr)_4\cdot(C_2H_2)$ (**10b**) (toluene-d_8, −40 °C)		187.3 ($^{13}C_2H_2$) ($J_{^{183}W-^{13}C}$ = 23.7 Hz, $^1J_{^{13}C-^{13}C}$ = 49 Hz, $^1J_{^{13}C-^1H}$ = 196, $^2J_{^{13}C-^1H}$ = 2 Hz)

pressure. For example, in **7a**, the bulky Me_3Si ligand on an α carbon atom of the μ-C_3 ligand causes the Me_3Si groups of the neighboring Me_3SiCH_2 ligands to be deflected away from it. This is shown in Figure 9 which provides a view of molecule **7a** looking down the W–W axis. The influence of the bulky Me_3Si substituent at the α carbon is passed on through the μ-$CSiMe_3$ ligand, which is canted to one side, to the Me_3SiCH_2 ligands on the other side of the molecule. The blades of the phenyl ligands at the α' and β positions of the μ-C_3 ligand are seen to take up positions of minimum steric hindrance. Similarly the position of the bulky Me_3Si ligand on the α carbon of the μ-C_3 ligand in **10a** results in understandable distortions in the W–C_α,C_α' distances to the μ-C_3 ligand. Also the W–O–C angles adjacent to the Me_3Si-substituted side of the μ-C_3 ligand are larger by 20° than those close to the H-substituted C_α' atom. A view looking down the W-to-W axis of molecule **10c** is shown in Figure 10.

Bonding in 7a and 10c. Valence Bond Description. The structural characterizations of **7a** and **10c** reveal that one tungsten atom in each molecule is essentially σ-bonded to the μ-C_3R_3 ligand, W(2) in both numbering schemes of the molecules, while the other tungsten atom, W(1), is π-bonded. It is therefore possible to partition the 3− charge of the C_3R_3 ligand as 2− to W(2) and −1 to W(1) and the μ-$CSiMe_3$ as 1− to W(2) and 2− to W(1). This results in a formal oxidation state of 5+ for both tungsten atoms, leading to the formalism that these compounds are d^1–d^1 dimers, W–W. The VB structure depicted in VIII below shows that W(2)

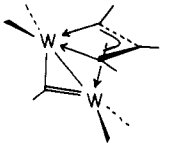

VIII

attains a share of 12 valence electrons and is in a square-based pyramidal geometry while W(1) attains a share of 14 valence electrons (4 from the π-allyl C_3R_3 ligand). The geometry about W(1) may be viewed as pseudotetrahedral if the μ-C_3R_3 ligand is considered to occupy one site.

There are some obvious limitations to this VB description. In particular, the W–C (μ-CMe_3) distances are essentially identical, indicating that the W–C single and double bond descriptions are not valid.

A cluster electron counting model for the $W_2(\mu\text{-}C_3R_3)$ moiety can be developed based on cluster electron pair counting rules.[23]

Table VII. Fractional Coordinates and Isotropic Parameters for $W_2(CH_2SiMe_3)_4(\mu\text{-}CSiMe_3)_2(\eta^2\text{-}PhCCMe)$

atom	10^4x	10^4y	10^4z	$10B_{iso}$
W(1)	2545 (1)	125 (1)	2838 (1)	24
W(2)	1240.5 (5)	77 (1)	2131 (1)	18
C(3)	2561 (28)	−338 (47)	4706 (32)	82 (15)
C(4)	2756 (20)	105 (39)	3915 (24)	53 (9)
C(5)	3290 (17)	411 (27)	3592 (20)	31 (7)
C(6)	3988 (21)	737 (34)	3760 (25)	46 (9)
C(7)	4408 (19)	653 (31)	3141 (22)	40 (8)
C(8)	5107 (21)	1011 (34)	3373 (26)	49 (9)
C(9)	5249 (27)	1173 (42)	4098 (32)	67 (12)
C(10)	4833 (27)	1251 (42)	4642 (31)	69 (13)
C(11)	4155 (20)	965 (33)	4486 (24)	45 (9)
C(12)	3033 (15)	−1257 (23)	2374 (18)	23 (6)
Si(13)	3300 (5)	−2450 (8)	2991 (6)	27 (2)
C(14)	2578 (15)	−3079 (24)	3480 (18)	22 (6)
C(15)	3596 (22)	−3477 (37)	2270 (27)	56 (10)
C(16)	3934 (21)	−2114 (34)	3696 (25)	47 (9)
C(17)	2819 (18)	1739 (30)	2446 (22)	36 (8)
Si(18)	2670 (5)	2985 (9)	2992 (7)	37 (2)
C(19)	3409 (20)	3516 (32)	3521 (24)	44 (9)
C(20)	1968 (31)	2873 (52)	3637 (36)	91 (17)
C(21)	2456 (29)	4020 (46)	2240 (34)	81 (15)
C(22)	1555 (15)	−39 (31)	3030 (18)	31 (6)
Si(23)	959 (4)	−179 (8)	3884 (5)	27 (2)
C(24)	969 (22)	−1535 (35)	4362 (26)	50 (10)
C(25)	969 (21)	981 (34)	4570 (25)	47 (9)
C(26)	129 (19)	−196 (34)	3426 (22)	48 (9)
C(27)	2976 (12)	5146 (22)	8287 (14)	14 (5)
Si(28)	2417 (5)	388 (8)	767 (6)	29 (2)
C(29)	1951 (16)	−473 (26)	38 (20)	29 (7)
C(30)	2301 (17)	1854 (29)	482 (21)	33 (7)
C(31)	3328 (21)	75 (41)	741 (24)	58 (10)
C(32)	663 (15)	−1211 (24)	1660 (19)	22 (6)
Si(33)	808 (5)	−2708 (8)	1736 (6)	27 (2)
C(34)	789 (19)	−3134 (32)	2719 (23)	43 (8)
C(35)	1608 (22)	−3089 (37)	1325 (27)	56 (10)
C(36)	88 (21)	−3470 (33)	1288 (26)	46 (9)
C(37)	810 (16)	1621 (26)	1978 (19)	27 (7)
Si(38)	189 (5)	1913 (8)	1228 (6)	32 (2)
C(39)	−644 (25)	1413 (42)	1467 (30)	67 (12)
C(40)	411 (18)	1348 (30)	329 (22)	37 (8)
C(41)	139 (20)	3436 (32)	1072 (24)	42 (9)

Table VIII. Selected Bond Distances for $W_2(\mu\text{-}CSiMe_3)_2(CH_2SiMe_3)_4\cdot[C_2(Me)(Ph)]$

A	B	distance, Å
W(1)	W(2)	2.915 (3)
W(1)	C(4)	1.97 (4)
W(1)	C(5)	2.04 (3)
W(1)	C(12)	2.15 (3)
W(1)	C(17)	2.19 (4)
W(1)	C(22)	2.06 (3)
W(1)	C(27)	2.26 (2)
W(2)	C(22)	1.73 (3)
W(2)	C(27)	1.78 (2)
W(2)	C(32)	2.14 (3)
W(2)	C(37)	2.11 (3)
Si(23)	C(22)	1.98 (3)
Si(28)	C(27)	1.92 (3)
C(3)	C(4)	1.58 (6)
C(4)	C(5)	1.30 (5)
C(5)	C(6)	1.50 (5)
Si	C(methyl)	1.88 (4) av
Si	C(methylene)	1.88 (4) av
C(Ar)	C(Ar)	1.40 (6) av

If the ligands are stripped from the W_2 center as μ-$CSiMe_3$, 3−, and CH_2SiMe_3 or O-*i*-Pr as each 1− and the μ-C_3R_3 ligand as 3−, the resultant W_2 center is formally 10+. Then each W center donates one electron for skeletal bonding. The $C_3R_3^{3-}$ fragment is broken down as follows: each CR unit donates 3 electrons to skeletal bonding; in addition there are 3 electrons because of its formal 3− charge, making a total of 12 electrons. The $W_2C_3R_3$ unit thus has a total of 14 skeletal electrons or 7 electron pairs for a 5-vertex bonding system. The cluster electron pair rule[23] predicts a nido structure, $n + 2 = 7$, for the central $W_2(\mu\text{-}C_3R_3)$ unit, IX.

Finally, it is worth examining the symmetrical form of the μ-C_3R_3 ligand depicted by X below and ask why this is not observed as the ground-state structure.

(23) Wade, K. *Adv. Inorg. Chem. Radiochem.* **1976**, *18*, 1.

Table IX. Selected Bond Angles for $W_2(\mu\text{-}CSiMe_3)_2(CH_2SiMe_3)_4[C_2(Me)(Ph)]$

A	B	C	angle, deg
C(4)	W(1)	C(5)	37.7 (14)
C(4)	W(1)	C(12)	106.1 (16)
C(4)	W(1)	C(17)	106.0 (17)
C(4)	W(1)	C(22)	91.7 (15)
C(4)	W(1)	C(27)	164.7 (13)
C(5)	W(1)	C(12)	92.9 (12)
C(5)	W(1)	C(17)	82.3 (14)
C(5)	W(1)	C(22)	128.4 (13)
C(5)	W(1)	C(27)	156.6 (11)
C(12)	W(1)	C(17)	118.3 (13)
C(12)	W(1)	C(22)	116.6 (13)
C(12)	W(1)	C(27)	82.8 (11)
C(17)	W(1)	C(22)	113.6 (14)
C(17)	W(1)	C(27)	79.6 (12)
C(22)	W(1)	C(27)	73.1 (11)
C(22)	W(1)	C(27)	94.7 (13)
C(22)	W(1)	C(32)	119.8 (15)
C(22)	W(1)	C(37)	109.9 (16)
C(27)	W(2)	C(32)	111.0 (12)
C(27)	W(2)	C(37)	105.9 (12)
C(32)	W(2)	C(37)	113.3 (13)
W(1)	C(4)	C(3)	146 (4)
W(1)	C(4)	C(5)	74.1 (25)
C(3)	C(4)	C(5)	137 (4)
W(1)	C(5)	C(4)	68.2 (24)
W(1)	C(5)	C(6)	150 (3)
C(4)	C(5)	C(6)	142 (4)
W(1)	C(12)	Si(13)	120.9 (16)
W(1)	C(17)	Si(18)	122.7 (19)
W(1)	C(22)	W(2)	100.4 (14)
W(1)	C(22)	Si(23)	138.9 (17)
W(2)	C(22)	Si(23)	120.6 (16)
W(1)	C(27)	W(2)	91.7 (10)
W(1)	C(27)	Si(28)	126.6 (12)
W(2)	C(27)	Si(28)	140.9 (15)
W(2)	C(32)	Si(33)	128.2 (17)
W(2)	C(37)	Si(38)	122.8 (18)

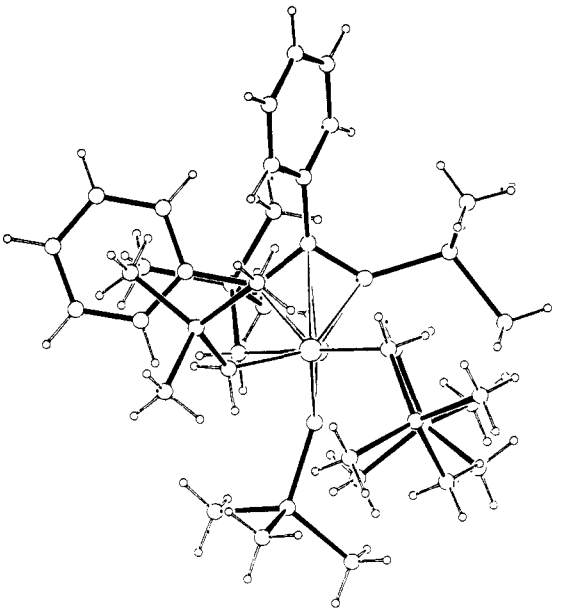

Figure 9. Ball-and-stick view of the $W_2(CH_2SiMe_3)_4(\mu\text{-}CSiMe_3)(\mu\text{-}CPhCPhCSiMe_3)$ molecule, **7a**, looking down the W–W axis.

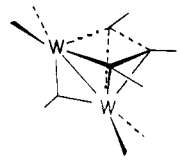

IX

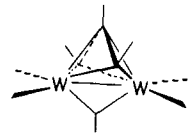

X

We believe the simplest answer is that neither tungsten atom can interact as strongly with the C_β atom as it would like. The W–C_β distance in X can be estimated, from a consideration of the structures found for **7a** and **10c**, to be ca. 2.5 Å. Energetically X may be viewed as the transition state for the interconversion of the VB isomers VIII.

NMR Studies on $W_2(\mu\text{-}CR^1CR^2CR^3)$-Containing Compounds. General Considerations. For the insertion compounds of formula $X_2W(\mu\text{-}CSiMe_3)(\mu\text{-}CR^1CR^2CR^3)WX_2$, the $X_2W(\mu\text{-}CSiMe_3)WX_2$ moiety provides a rigid template. It is not stereochemically labile on the NMR time scale. (1) The methylene protons of the CH_2SiMe_3 ligands and the methyl groups of the O-*i*-Pr ligands are diastereotopic in the temperatue range −80 to +100 °C. (2) The μ-$CSiMe_3$ ligand does not exchange on the NMR time scale with the $CSiMe_3$ group incorporated in the μ-$CR^1CR^2CR^3$ ligand.

The X_2WWX_2 moiety provides a probe for the symmetry of the μ-$CR^1CR^2CR^3$ ligand. If the substituents on the α and α' carbon atoms, R^1 and R^3, are equivalent, then a consideration of the observed structures for **7a** and **10c** leads to the expectation of two types of X groups, X_2WWX_2'. However, when X = CH_2SiMe_3, this situation is never realized even at low temperatures: all four CH_2SiMe_3 ligands are equivalent. Evidently the μ-C_3R_3 ligand is hopping backward and forward passing through the symmetrical structure X very rapidly.

When the substituents on α and α', R^1 and R^3, are not equivalent, then the molecule lacks a plane of symmetry containing the W–W axis, and spectra reveal an XX′WWXX′ moiety.

Only in the case of the isopropoxy compound **10c**, $W_2(O\text{-}i\text{-}Pr)_4(\mu\text{-}CSiMe_3)(\mu\text{-}CHCHCSiMe_3)$, at low temperature, <−70 °C, is there evidence in the NMR spectra for the freezing out of the ground-state structure of the $W_2(\mu\text{-}C_3R_3)$ moiety. The OC*H*Me_2 signals appear as four broad resonances of equal intensity at −80 °C, but on raising the temperature, these collapse in a pairwise manner to give two sharp septets at ambient temperatures.

The assignment of the groups within the μ-$CR^1CR^2CR^3$ ligand follows from the following considerations. (1) The ^{13}C NMR spectra identify the C_α and C_α' carbon atoms by their coupling to ^{183}W, $J_{^{183}W\text{-}^{13}C}$ ca. 30 Hz. No coupling to ^{183}W has been observed to the C_β atom. (2) Proton-coupled ^{13}C NMR spectra identify CH units within the μ-C_3 ligand. (3) The symmetry within the μ-C_3 ligand is reflected by the resonances of the X_2WWX_2 moiety as noted above.

An empirical relationship between C*H* ^1H signals for the μ-allyl group emerges from the above. Within the μ-C_3 ligand, H atoms attached to either α or α' (R^1 or R^3 = H) appear at ca. 6 ppm while those attached to the β carbon atoms (R^2 = H) appear at ca. 9 ppm. Applying this empirical rule to the three isomers derived from the insertion of PhC≡CH into a μ-$CSiMe_3$ ligand, it is possible to identify the isomer having the H atom attached to the β carbon atom (**8a**) in the presence of the other two structural isomers (**8c** and **8d**). Above −20 °C, **8a** and **8c** interconvert readily on the NMR time scale. This strongly suggests that **8c** is the isomer having a H atom attached to the α carbon atom and a Ph group on the β carbon atom because an exchange process involving C–H and C–Ph units should have a small activation energy compared to similar processes involving the interchange of a C–H and C–$SiMe_3$ ligand (see section Dynamic Processes Involving μ-C_3R_3 Ligand below).

For products derived from insertion reactions involving disubstituted alkynes, assignments of the *CR* resonances (^1H and ^{13}C) are inferred from their chemical shift positions with respect to similar substituents derived from monosubstituted acetylenes, RCCH.

Table X. Fractional Coordinates and Isotropic Parameters for $W_2(CH_2SiMe_3)_4(\mu\text{-}CSiMe_3)(\mu\text{-}CPhCPhCSiMe_3)$

atom	10^4x	10^4y	10^4z	$10B_{iso}$
W(1)	9362.5 (2)	−621.4 (3)	−129.5 (3)	11
W(2)	9525.7 (2)	1195.4 (3)	101.1 (3)	11
C(3)	11392 (7)	−189 (11)	778 (8)	19
C(4)	11803 (7)	−409 (12)	1416 (9)	24
C(5)	11551 (7)	−605 (13)	2160 (9)	26
C(6)	10890 (7)	−543 (13)	2276 (8)	25
C(7)	10498 (7)	−322 (10)	1648 (8)	19
C(8)	10727 (6)	−149 (9)	894 (7)	14
C(9)	10285 (5)	91 (10)	225 (7)	15
C(10)	10387 (6)	29 (10)	−604 (7)	16
C(11)	939 (6)	9536 (10)	8985 (7)	15
C(12)	11334 (7)	107 (14)	−1518 (9)	29
C(13)	11849 (8)	−319 (18)	−1903 (12)	43
C(14)	11994 (9)	−1271 (20)	−1776 (10)	47
C(15)	11616 (8)	−1852 (13)	−1281 (12)	35
C(16)	11111 (7)	−1430 (11)	−896 (9)	22
C(17)	9849 (6)	461 (10)	−965 (7)	13
Si(18)	9690 (2)	695 (3)	−2034 (2)	16
C(19)	9929 (7)	−323 (11)	−2682 (8)	21
C(20)	10157 (7)	1807 (11)	−2354 (9)	24
C(21)	8817 (7)	942 (12)	−2208 (9)	24
C(22)	9486 (6)	−1751 (10)	701 (7)	16
Si(23)	9882 (2)	−2955 (3)	625 (2)	22
C(24)	9928 (8)	−3461 (11)	−400 (9)	26
C(25)	9376 (10)	6201 (12)	1208 (11)	41
C(26)	10697 (11)	−2887 (13)	1062 (12)	40
C(27)	8920 (6)	−1298 (9)	−1124 (8)	16
Si(28)	8089 (2)	−1840 (3)	−1089 (2)	20
C(29)	7982 (7)	−2806 (11)	−300 (9)	24
C(30)	7929 (7)	7554 (13)	7929 (9)	24
C(31)	7501 (7)	−833 (11)	−925 (9)	22
C(32)	8801 (6)	317 (9)	410 (8)	15
Si(33)	8177 (2)	300 (3)	1203 (2)	16
C(34)	7896 (7)	−970 (12)	1443 (10)	25
C(35)	8553 (7)	823 (12)	2116 (8)	25
C(36)	7438 (7)	982 (13)	914 (10)	29
C(37)	9963 (7)	1878 (11)	1108 (8)	20
Si(38)	10685 (2)	2627 (3)	916 (2)	19
C(39)	11251 (8)	2418 (14)	1780 (9)	29
C(40)	10468 (8)	3918 (12)	894 (12)	35
C(41)	11086 (6)	2304 (11)	−29 (9)	24
C(42)	9286 (7)	2480 (9)	−561 (9)	20
Si(43)	8551 (2)	3203 (3)	−334 (2)	17
C(44)	8422 (8)	3399 (13)	761 (9)	26
C(45)	7835 (7)	2618 (13)	−784 (9)	25
C(46)	8637 (8)	4440 (12)	−772 (10)	29

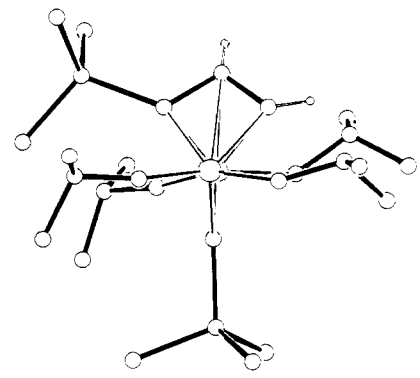

Figure 10. Ball-and-stick view of the $W_2(O\text{-}i\text{-}Pr)_4(\mu\text{-}CSiMe_3)(\mu\text{-}CHCHCSiMe_3)$ molecule, **10c**, looking down the W–W axis.

Table XI. Fractional Coordinates and Isotropic Parameters for $W_2(O\text{-}i\text{-}Pr)_4(\mu\text{-}CSiMe_3)(\mu\text{-}CHCHCSiMe_3)$

atom	10^4x	10^4y	10^4z	$10B_{iso}$
W(1)	2118.0 (2)	33.0 (3)	7624.7 (4)	14
W(2)	3409.6 (2)	375.0 (2)	6923.4 (4)	13
C(3)	3038 (6)	970 (6)	8436 (11)	15
C(4)	3084 (6)	416 (6)	9422 (10)	14
C(5)	3300 (6)	−225 (6)	8717 (10)	15
Si(6)	3636 (2)	−1127 (2)	9639 (3)	17
C(7)	3129 (7)	−1255 (7)	11003 (11)	25
C(8)	3424 (7)	−1923 (6)	8400 (12)	21
C(9)	4695 (7)	−1077 (7)	10560 (13)	27
C(10)	2361 (6)	69 (6)	5850 (11)	17
Si(11)	1796 (2)	−90 (2)	4025 (3)	23
C(12)	1854 (8)	−1089 (8)	3553 (13)	32
C(13)	2203 (10)	491 (9)	2840 (14)	47
C(14)	769 (9)	180 (10)	3825 (17)	54
O(15)	1625 (4)	−865 (4)	7753 (8)	22
C(16)	1382 (7)	−1588 (6)	8017 (12)	23
C(17)	803 (8)	−1498 (8)	8887 (15)	38
C(18)	1017 (9)	−1979 (8)	6665 (14)	38
O(19)	1348 (4)	755 (5)	7673 (7)	22
C(20)	1224 (6)	1372 (8)	8462 (14)	33
C(21)	624 (10)	1145 (10)	9201 (16)	53
C(22)	987 (12)	2016 (11)	7590 (26)	77
O(23)	3658 (4)	1303 (4)	6265 (7)	19
C(24)	3622 (7)	2091 (7)	6482 (12)	24
C(25)	4219 (8)	2475 (7)	5951 (13)	32
C(26)	2806 (8)	2353 (8)	5808 (16)	38
O(27)	4178 (4)	−243 (4)	6580 (8)	19
C(28)	4658 (6)	−871 (6)	6645 (11)	21
C(29)	5477 (7)	−673 (8)	6689 (13)	30
C(30)	4266 (9)	−1396 (8)	5478 (17)	47

Table XII. Selected Bond Distances for $W_2[\mu\text{-}C(Ph)C(Ph)C(SiMe_3)](\mu\text{-}CSiMe_3)(CH_2SiMe_3)_4$

A	B	distance, Å
W(1)	W(2)	2.548 (1)
W(1)	C(9)	2.24 (1)
W(1)	C(10)	2.45 (1)
W(1)	C(17)	2.29 (1)
W(1)	C(22)	2.10 (1)
W(1)	C(27)	2.13 (1)
W(1)	C(32)	1.96 (1)
W(2)	C(9)	2.20 (1)
W(2)	C(10)	2.68 (1)
W(2)	C(17)	2.17 (1)
W(2)	C(32)	2.00 (1)
W(2)	C(37)	2.14 (1)
W(2)	C(42)	2.15 (1)
Si(18)	C(17)	1.86 (1)
Si(33)	C(32)	1.87 (1)
C(8)	C(9)	1.49 (2)
C(9)	C(10)	1.41 (2)
C(10)	C(11)	1.51 (2)
C(10)	C(17)	1.41 (2)
Si	C(Me)	1.87 (2) av
C(Ar)	C(Ar)	1.39 (2) av

The only ambiguities which may arise involve the latter assumption, i.e., relate to the assignment of $\mu\text{-}CR^1CR^2CR^3$ ligands where all the substituents are different and none is a hydrogen atom. Also, an absolute assignment of X and X′ is not possible when the substituents R^1 and R^3 differ. This ambiguity is inconsequential in determining the structure of the overall molecule.

Dynamic Processes Involving the μ-C_3R_3 Ligand. Two dynamic processes have been identified relating to the μ-C_3R_3 ligand. The first and lowest energy process involves the flipping back and forth of the allyl via the symmetrical transition state X. This process makes the two tungsten atoms equivalent and is a very low-energy process, less than ca. 8 kcal mol^{-1}, having only been frozen out in one instance. The other processes are higher energy processes involving C_α/C_β site exchange and C_α/C_α' site exchange.

C_α/C_β Site Exchange. The ^1H NMR spectra for the compound **5a** reveals that the signals associated with the CMe groups of the

Table XIII. Bond Distances for $W_2[\mu\text{-}C(H)C(H)C(SiMe_3)](\mu\text{-}CSiMe_3)(O\text{-}i\text{-}Pr)_4$

A	B	distance, Å
W(1)	W(2)	2.658 (1)
W(1)	O(15)	1.851 (8)
W(1)	O(19)	1.894 (8)
W(1)	C(3)	2.33 (1)
W(1)	C(4)	2.23 (1)
W(1)	C(5)	2.14 (1)
W(1)	C(10)	1.94 (1)
W(2)	O(23)	1.883 (7)
W(2)	O(27)	1.865 (7)
W(2)	C(3)	2.10 (1)
W(2)	C(4)	2.72 (1)
W(2)	C(5)	2.15 (1)
W(2)	C(10)	1.96 (1)
Si(11)	C(10)	1.85 (1)
C(3)	C(4)	1.38 (2)
C(4)	C(5)	1.45 (2)
Si	C(methyl)	1.86 av
O	C	1.41 av

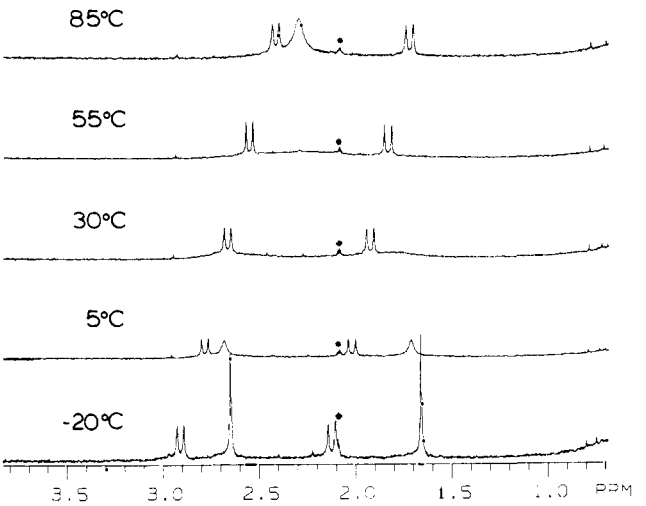

Figure 11. ^1H NMR spectra of $W_2(CH_2SiMe_3)_4(\mu\text{-}CSiMe_3)(\mu\text{-}CMeCMeCSiMe_3)$, **5a**, showing the μ-C*Me*C*Me*$CSiMe_3$ signals as a function of temperature. Two parts of AX patterns associated with the terminal CH_2SiMe_3 ligands are also shown.

μ-$CMeCMeCSiMe_3$ ligand undergo site exchange on the NMR time scale. See Figure 11. The CMe group scrambling does not create an apparent mirror plane in the molecule as there remain two types of Me_3SiCH_2 ligands characteristic of an XX′WWXX′ template bearing a μ-C_3 ligand with $R^1 \neq R^3$.

In the insertion reaction between HCCH and **1**, the kinetically formed product is **3c** containing the μ-$CHCHCSiMe_3$ ligand. The signals associated with the α and β CH protons appear at ca. 6 and 9 ppm, respectively, which upon warming from −40 to −10 °C start to broaden and collapse into the base line. At higher temperatures a rearrangement to the thermodynamic product **3a** containing the μ-$CHCSiMe_3CH$ ligand occurs which precludes observing a rapid C_α/C_β exchange on the NMR time scale.

Another interesting example of site exchange within the C_3R_3 ligand is seen in high-temperature spectra of **9a**, $W_2(CH_2SiMe_3)_4(CSiMe_3)(\mu\text{-}CHCSiMe_3CSiMe_3)$. At low temperatures, there are signals corresponding to two types of Me_3SiCH_2 ligands as expected for an XX′WWXX′ template supported as μ-$CR^1CR^2CR^3$ ligand, where $R^1 \neq R^3$. Also, since R^1 = H, R^2 = $SiMe_3$, and R^3 = $SiMe_3$, there are two $SiMe_3$ signals associated with the μ-C_3R_3 ligand. When the temperature is raised to >80 °C, the two $SiMe_3$ signals associated with the μ-allyl ligand collapse to a single signal and the two types of Me_3SiCH_2 ligands become averaged on the NMR time scale. The fluxional process generates an apparent plane of symmetry containing the W–W axis. Site exchange between R^1 = H and R^2 = $SiMe_3$ could produce the μ-$CSiMe_3CHCSiMe_3$-containing isomer. Now R^1

Table XIV. Selected Bond Angles for $W_2[\mu\text{-}C(Ph)C(Ph)C(SiMe_3)](\mu\text{-}CSiMe_3)(CH_2SiMe_3)_4$

A	B	C	angle, deg
W(2)	W(1)	C(9)	54.4 (3)
W(2)	W(1)	C(10)	64.9 (3)
W(2)	W(1)	C(17)	52.9 (3)
W(2)	W(1)	C(22)	127.2 (4)
W(2)	W(1)	C(27)	127.3 (4)
W(2)	W(1)	C(32)	50.7 (4)
C(9)	W(1)	C(10)	34.7 (4)
C(9)	W(1)	C(17)	59.9 (4)
C(9)	W(1)	C(22)	92.3 (5)
C(9)	W(1)	C(27)	140.7 (5)
C(9)	W(1)	C(32)	96.0 (5)
C(9)	W(1)	C(17)	34.4 (4)
C(10)	W(1)	C(22)	112.2 (5)
C(10)	W(1)	C(27)	106.4 (4)
C(10)	W(1)	C(32)	115.6 (5)
C(17)	W(1)	C(22)	146.6 (5)
C(17)	W(1)	C(27)	89.6 (5)
C(17)	W(1)	C(32)	97.1 (5)
C(22)	W(1)	C(27)	104.7 (5)
C(22)	W(1)	C(32)	104.5 (5)
C(27)	W(1)	C(32)	113.0 (5)
W(1)	W(2)	C(9)	55.7 (3)
W(1)	W(2)	C(10)	55.8 (3)
W(1)	W(2)	C(17)	57.3 (3)
W(1)	W(2)	C(32)	49.4 (4)
W(1)	W(2)	C(37)	127.3 (4)
W(1)	W(2)	C(42)	134.0 (4)
C(9)	W(2)	C(10)	31.7 (4)
C(9)	W(2)	C(17)	62.2 (5)
C(9)	W(2)	C(32)	96.0 (5)
C(9)	W(2)	C(37)	85.4 (5)
C(9)	W(2)	C(42)	141.5 (5)
C(10)	W(2)	C(17)	31.5 (4)
C(10)	W(2)	C(32)	105.2 (5)
C(10)	W(2)	C(37)	109.0 (5)
C(10)	W(2)	C(42)	114.7 (5)
C(17)	W(2)	C(32)	99.8 (5)
C(17)	W(2)	C(37)	136.6 (5)
C(17)	W(2)	C(42)	91.4 (5)
C(32)	W(2)	C(37)	112.3 (6)
C(32)	W(2)	C(42)	116.9 (5)
C(37)	W(2)	C(42)	98.7 (6)
W(1)	C(9)	W(2)	69.9 (3)
W(1)	C(9)	C(8)	129.5 (9)
W(1)	C(9)	C(10)	80.8 (7)
W(2)	C(9)	C(8)	131.9 (9)
W(2)	C(9)	C(10)	93.2 (8)
C(8)	C(9)	C(10)	129.7 (12)
W(1)	C(10)	W(2)	59.3 (3)
W(1)	C(10)	C(9)	64.5 (6)
W(1)	C(10)	C(11)	130.9 (10)
W(1)	C(10)	C(17)	66.4 (6)
W(2)	C(10)	C(9)	55.1 (7)
W(2)	C(10)	C(11)	169.9 (10)
W(2)	C(10)	C(17)	53.5 (6)
C(9)	C(10)	C(11)	126.5 (11)
C(9)	C(10)	C(17)	106.4 (11)
C(11)	C(10)	C(17)	127.0 (10)
W(1)	C(17)	W(2)	69.8 (3)
W(1)	C(17)	Si(18)	129.0 (6)
W(1)	C(17)	C(10)	79.3 (7)
W(2)	C(17)	Si(18)	131.8 (7)
W(2)	C(17)	C(10)	95.0 (8)
Si(18)	C(17)	C(10)	129.3 (9)
W(1)	C(32)	W(2)	79.9 (4)
W(1)	C(32)	Si(33)	137.6 (7)
W(2)	C(32)	Si(33)	136.1 (8)

Table XV. Bond Angles for $W_2[\mu\text{-}C(H)C(H)C(SiMe_3)](\mu\text{-}CSiMe_3)(O\text{-}i\text{-}Pr)_4$

A	B	C	angle, deg
W(2)	W(1)	O(15)	132.9 (2)
W(2)	W(1)	O(19)	122.4 (2)
W(2)	W(1)	C(3)	49.4 (2)
W(2)	W(1)	C(4)	67.1 (3)
W(2)	W(1)	C(5)	51.8 (3)
W(2)	W(1)	C(10)	47.3 (3)
O(15)	W(1)	O(19)	103.1 (3)
O(15)	W(1)	C(3)	154.4 (4)
O(15)	W(1)	C(4)	119.1 (4)
O(15)	W(1)	C(5)	101.4 (4)
O(15)	W(1)	C(10)	108.9 (4)
O(19)	W(1)	C(3)	86.9 (4)
O(19)	W(1)	C(4)	100.0 (4)
O(19)	W(1)	C(5)	138.8 (4)
O(19)	W(1)	C(10)	110.3 (4)
C(3)	W(1)	C(4)	35.3 (4)
C(3)	W(1)	C(5)	58.5 (4)
C(3)	W(1)	C(10)	89.0 (4)
C(4)	W(1)	C(5)	38.8 (4)
C(4)	W(1)	C(10)	114.3 (4)
C(5)	W(1)	C(10)	92.2 (4)
W(1)	W(2)	O(23)	126.9 (2)
W(1)	W(2)	O(27)	130.3 (2)
W(1)	W(2)	C(3)	57.1 (3)
W(1)	W(2)	C(5)	51.5 (3)
W(1)	W(2)	C(10)	46.9 (3)
O(23)	W(2)	O(27)	101.6 (3)
O(23)	W(2)	C(3)	87.7 (4)
O(23)	W(2)	C(5)	144.9 (4)
O(23)	W(2)	C(10)	109.5 (4)
O(27)	W(2)	C(3)	145.8 (4)
O(27)	W(2)	C(5)	95.8 (4)
O(27)	W(2)	C(10)	111.8 (4)
C(3)	W(2)	C(5)	61.9 (4)
C(3)	W(2)	C(10)	95.4 (4)
C(5)	W(2)	C(10)	91.5 (4)
W(1)	O(15)	C(16)	169.4 (7)
W(1)	O(19)	C(20)	140.8 (7)
W(2)	O(23)	C(24)	142.1 (7)
W(2)	O(27)	C(28)	159.4 (7)
W(1)	C(3)	W(2)	73.5 (3)
W(1)	C(3)	C(4)	68.4 (6)
W(2)	C(3)	C(4)	100.6 (8)
W(1)	C(4)	C(3)	76.3 (6)
W(1)	C(4)	C(5)	67.3 (6)
C(3)	C(4)	C(5)	100.9 (9)
W(1)	C(5)	W(2)	76.6 (3)
W(1)	C(5)	Si(6)	125.0 (5)
W(1)	C(5)	C(4)	73.9 (6)
W(2)	C(5)	Si(6)	138.8 (6)
W(2)	C(5)	C(4)	96.4 (7)
W(1)	C(10)	W(2)	85.8 (4)
W(1)	C(10)	Si(11)	134.5 (6)
W(2)	C(10)	Si(11)	139.6 (6)
W(1)	C(3)	H(2)	112.0 (7)
W(2)	C(3)	H(2)	140.0 (7)
C(4)	C(3)	H(2)	119.0 (7)
W(1)	C(4)	H(1)	115.0 (6)
C(5)	C(4)	H(1)	132.0 (7)

$= R^3 = SiMe_3$, and a return to the thermodynamically favored isomer having H in either the α or α' positions would occur. It is also possible to invoke an α/α' exchange ($CR^1 \rightleftharpoons CR^3$) site exchange to generate the mirror plane directly, though this does not exchange the α and β $SiMe_3$ groups in this instance.

We propose a general scheme which encompasses all the rearrangements observed involving the formation of a $W_2(\mu$-η^1,η^2-cyclopropene) intermediate, by formation of a carbon–carbon bond between the α and α' carbons of the allyl moiety. Then by a sequence of 60° rotations followed by C–C bond openings, all possible isomers of the ground-state μ-$CR^1CR^2CR^3$ ligand are accessible. These rearrangements are shown in Scheme II.

The reader should note that one can rigorously rule out a rapid reversible deinsertion of an alkyne from the μ-$CR^1CR^2CR^3$ ligand as an explanation for both the fluxional processes and the rearrangements within the μ-C_3R_3 ligand. (1) The activation energy for the insertion process for the reaction involving MeCCMe is $\Delta G^\dagger = 25$ kcal mol^{-1} and $\Delta G^\dagger$ for the back reaction must be larger. In contrast the activation energy for the rearrangement process is 15 kcal mol^{-1}. (2) A reversible deinsertion would scramble the $CSiMe_3$ group of the μ-allyl ligand and the bridging alkylidyne

Table XVI. Stereochemistry of the Kinetic and Thermodynamic Products of Alkyne Insertion Involving **1**

alkyne	kinetic prod	thermodynamic prod		
HCCH	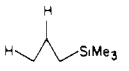	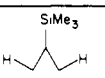		
HCCPh	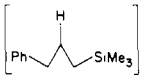	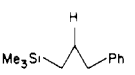	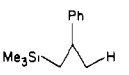	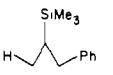
HCCMe	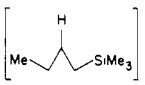	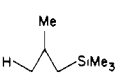		
$HCCSiMe_3$	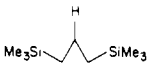	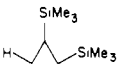		
MeCCMe		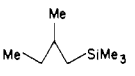		
MeCCPh		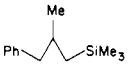		
PhCCPh		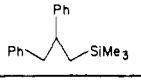		

ligand. In the case of the compound **5a**, deinsertion would also create an additional molecular plane of symmetry, thereby generating one time-averaged type of CH_2SiMe_3 ligand. None of these are observed.

The energies of activation for interconverting the various isomers are presumably largely determined by steric factors both in the ground state and transition states. Steric factors are also presumably the predominant factors in favoring the thermodynamic site preferences within the μ-$CR^1CR^2CR^3$ products described. Electronic factors may also contribute in a way which we do not presently understand. For example, it is difficult to reconcile the favored formation of the μ-$CHCSiMe_3CH$ ligand in the reaction between **1** and CH≡CH on either steric or electronic grounds when the reaction between **1** and MeC≡CH leads to μ-$CHCMeCSiMe_3$. A summary of the stereochemistry of the insertion products is shown in Table XVI.

Mechanistic Considerations Pertaining to the Insertion Reaction.[24] **General Considerations.** Most of our studies have involved the Me_3SiCH_2 ligated compound **1**, but the limited data obtained from studies of **2**, the isoproxy compound, suggest a common reaction pathway. Qualitatively, the rates of insertion into the μ-$CSiMe_3$ ligand in **1** follow the order RC≡CH > RC≡CR′. In the case of the disubstituted alkynes, MeC≡CMe and PhC≡CMe, simple 1:1 alkyne adducts can be isolated. In all the cases for RC≡CH (R = H, Me, Me_3Si, *t*-Bu, and Ph), initial formation of 1:1 alkyne adducts is seen to be rapid at low temperatures by NMR studies. Within the series of terminal alkyne adducts, the rate of insertion follows the series HC≡CH ~ Me_3SiC≡CH > MeC≡CH > *t*-BuC≡CH > PhC≡CH. The relative rates span roughly 1 order of magnitude compared to the 3–4 orders of magnitude difference observed between the disubstituted and monosubstituted compounds.

A number of factors identify the alkyne adducts as intermediates in the insertion reaction. For example, when the dimethylacetylene adduct **5b** was dissolved in benzene-d_6 and exposed to an excess of C_2H_2 at room temperature, no formation of the ethyne insertion product was observed. Also, as shown below, alkyne adducts show first-order rate behavior in the formation of the μ-allyl compounds.

Studies of Reaction Kinetics. The reactions between **1** and each of MeC≡CMe and Me_3SiC≡CH were followed by NMR spectroscopy as a function of time. The initially formed alkyne adducts were seen to react to give the insertion products, and the reactions were followed for three or more half-lives and at four temperatures in the range −30 to −5 °C for reactions involving Me_3SiC≡CH and from 35 to 80 °C for MeC≡CMe. In these reactions, the rate of formation of the μ-C_3R_3 compounds was dependent only on the concentration of the alkyne adducts to the

Scheme II. General Scheme for the Rearrangement of the μ-CRCR′CR″ Ligand in $W_2(CH_2SiMe_3)_4(\mu\text{-}CSiMe_3)(\mu\text{-}CRCR'CR'')$ Compounds through the Formation of a μ-CRCR′CR″ Cyclopropenyl Intermediate[a]

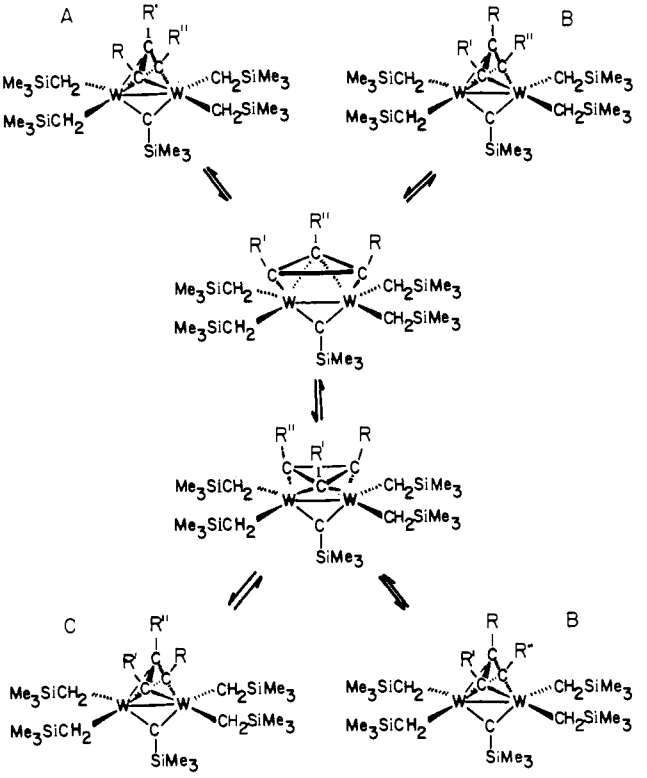

[a] The α–β exchange route is shown by the A and B interconversion at the top. The hypothetical α–α' site exchange is illustrated by the A and C interconversion. All site exchanges of CR, CR′, and CR″ are accessible by successive 60° rotations of the μ-cyclopropenyl intermediates.

(24) Nomenclature: The formation of the μ-$CR^1CR^2CR^3$ ligand is generally referred to as an "insertion reaction in whis work. This term is derived from the classical "migratory insertion" reaction common to coordination chemistry, in which a ligand bound to a metal center moves from its coordination site, inserting into a metal–ligand bond at another coordination site. The formation of the μ-allyl ligand in this work can also be correctly defined as a cycloaddition or ring-expansion reaction.

Scheme III. Pictorial Representation of a Proposed Mechanism of Alkyne Insertion into the μ-CSiMe$_3$ Ligand[a]

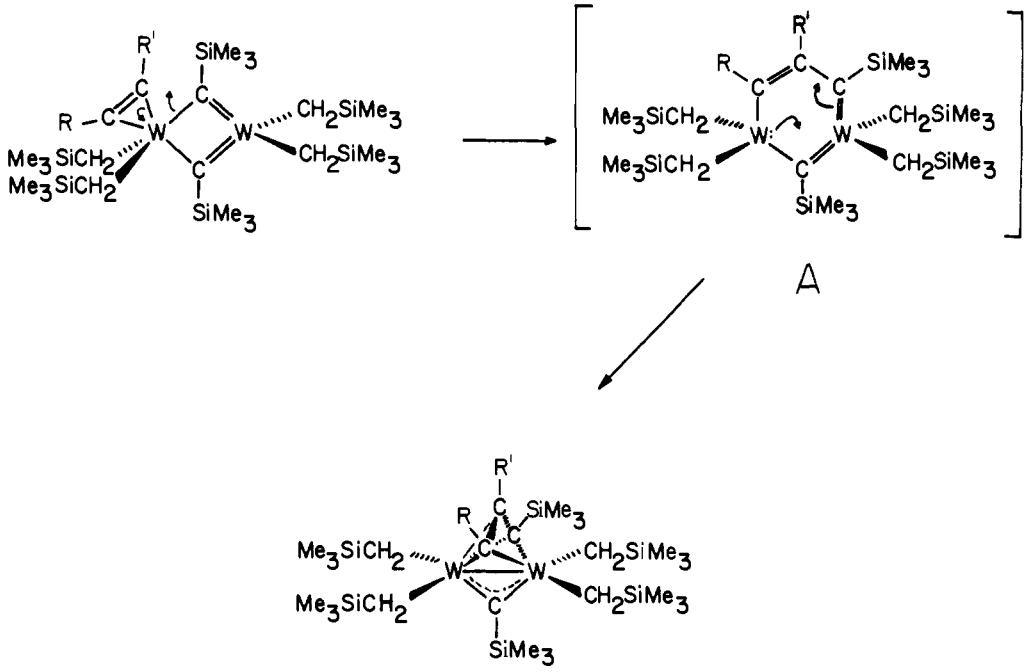

[a] Double-headed arrows show formal electron-pair motion during the formation of the activated complex "A" and the final rearrangement to the μ-CRCR'CSiMe$_3$ ligand. The stereochemistry shown for "A" represents only that C–C bond formation is occurring with an intact alkyne unit involving the carbon atom bearing the least sterically bulky substituent.

first power and the temperature.

A reasonable determination of the activation parameters $\Delta H^{\dagger}$ and $\Delta S^{\dagger}$ was made based on these studies. For reactions involving the MeC$_2$Me adduct, $\Delta H^{\dagger}$ = 20.4 ± 0.7 kcal mol^{-1} and $\Delta S^{\dagger}$ = −13 ± 2 eu, while for the Me$_3$SiCCH adduct $\Delta H^{\dagger}$ = 15.2 ± 1.2 kcal mol^{-1} and $\Delta S^{\dagger}$ = −15 ± 5 eu.

The level of accuracy for studies involving Me$_3$SiC≡CH was poorer due to the difficulties in sample handling and low temperature control. This not withstanding, the activation parameters present a consistent picture. The greater rate of reaction, Me$_3$SiC≡CH > MeC≡CMe, is seen to be due to the lower enthalpy of activation. In both reactions, the entropy of activation is negative and of medium magnitude. This is readily interpretable in terms of an intramolecular reaction involving a highly ordered transition state.

Stereochemistry Involving C–C Bond Formation. Careful studies of these reactions at low temperatures show that the kinetically formed product always contains an intact C$_2$ unit derived from the alkyne, i.e., the acetylenic carbons occupy the α and β positions. This is clearly seen in the ^{13}C NMR spectrum of the initially formed insertion product **3c** in the reaction between **1** and H*C≡*CH, where *C represents 92.5 atom % ^{13}C, as shown in Figure 12. A subsequent rearrangement to the thermodynamic product **3a** containing the μ-CHCSiMe$_3$CH ligand is rapid, however. This presents a picture of the insertion step as one involving C–C bond formation between a carbon atom of the coordinated alkyne and the μ-CSiMe$_3$ carbon.

The relative rates of reaction indicate that steric factors are particularly important in the C–C bond-forming step: $k_{RC\equiv CH} > k_{RC\equiv CR}$. It seems likely that the methyne carbon atom of the alkyne is the one which initially is involved in forming the new C–C bond. However, all the studies of the insertion reaction involving **1** and MeC≡CH and Me$_3$SiC≡CH showed that the first detectable product had the Me or Me$_3$Si substituent in the β position. In reactions involving **1** and PhC≡CH, a mixture of isomers is formed containing the Ph substituent at both the α and β positions of the μ-C$_3$R$_3$ ligand. However, in the reaction between the isopropoxy compound **2** and Me$_3$SiC≡CH, the kinetic product is seen to be W$_2$(O-*i*-Pr)$_4$(μ-CSiMe$_3$)(μ-CSiMe$_3$CHCSiMe$_3$) which upon heating rearranges to the less symmetrical product W$_2$(O-*i*-Pr)$_4$(μ-CSiMe$_3$)(μ-CHCSiMe$_3$CSiMe$_3$), containing the bulky SiMe$_3$ substituent in the β position.

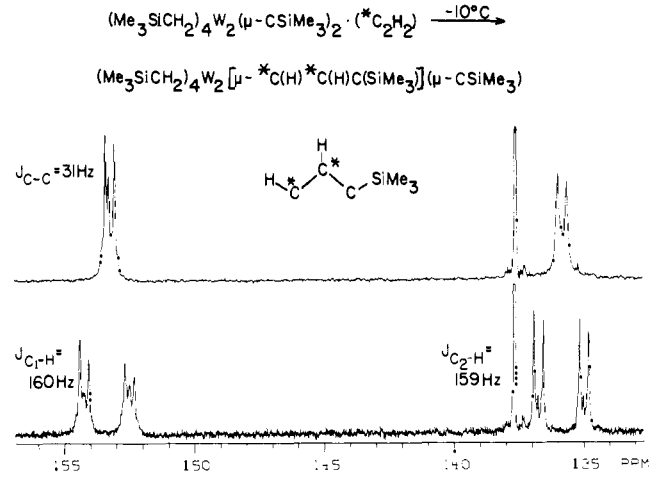

Figure 12. ^{13}C NMR spectra of W$_2$(CH$_2$SiMe$_3$)$_4$(μ-CSiMe$_3$)(μ-*CH*CHCSiMe$_3$), **3c**, where *C represents 92.5 atom % ^{13}C enrichment, showing the μ-*CH*CHCSiMe$_3$ signals, at −10 °C in toluene-d_8 at 90.8 MHz. The spectrum shown at the top is proton-decoupled and at the bottom is proton-coupled. The quaternary aromatic carbon resonance of toluene-d_8 solvent occurs at ca. 138 ppm.

We suggest that both **1** and **2** have a common reaction pathway in their reactions with alkynes differing only in the relative energetics of the intermediates and transition states. This leads to our proposal of initial alkyne adduct formation followed by insertion, eq I. In all cases, the initial C–C bond formation involves the least sterically substituted end of the alkyne, e.g., CH for RC≡CH. However, in the case of X = CH$_2$SiMe$_3$, the energy of activation for α/β site exchange (see earlier section) is less than the energy of activation for insertion, leading to the nondetection of the kinetic insertion products. In the case of X = O-*i*-Pr, the activation energy for α/β site exchange is higher than that for X = CH$_2$SiMe$_3$ and more importantly higher than that for the insertion process. Consequently, it is possible to detect and even isolate kinetic products of insertion prior to α/β site exchange reactions involving the μ-CR^{1}CR^{2}CR^3 ligand.

The insertion reaction is represented by the sequence shown in Scheme III. There is no stereochemical implication intended

Scheme IV. Pictorial Representation of an Alternate Mechanism of Alkyne Insertion, Featuring a More Oblique Attack of the Coordinated Alkyne on the Bridging Alkylidyne Ligand[a]

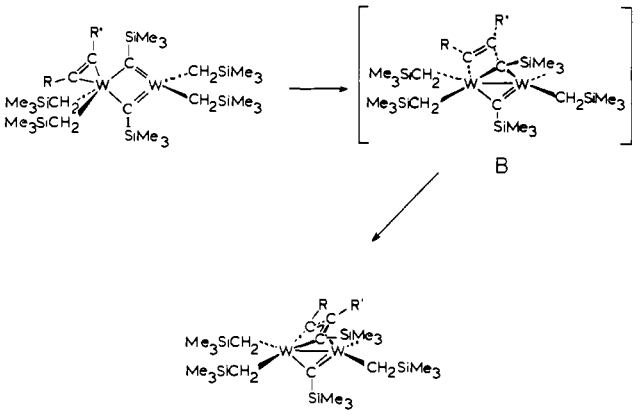

[a] The activated complex "B", which features approximate tetrahedral stereochem stry at the alkylidyne carbon, rearranges with relatively minor atomic motion to form the μ-CRCR'CSiMe$_3$ ligand. All the mechanistic features satisfied by the proposal presented in Scheme III are also encompassed by this model. (The fourth Me_3SiCH_2 group has been omitted in "B" and the final product for the sake of clarity.)

by our sketch of the activated complex with respect to planarity of the central six-membered ring. The valence bond description and use of arrows denoting electron pair motion is consistent with the VB descriptions developed for the initial adduct and final product. In particular, it is useful to see that the migratory insertion reaction regenerates the W–W bond. The reader may find the stereochemical pathway depicted in Scheme IV more appealing. Finally, we note that the scheme represents C–C bond formation in a one-on-one manner. Our results rule out a crosswise addition of the alkyne to the metal–alkylidyne carbon.

Comparison with Related Studies. Structural analogues of the 1,3-dimetallaallyl insertion products have been observed by Stone and co-workers[25,26] from reactions between alkynes and μ_2-alkylidyne bridged W–Fe and W–Co compounds. The central core of the Cp(CO)$_2$W[μ-C(Me)C(Me)C(*p*-tolyl)]Fe(CO)$_3$ molecule takes up a square-based pyramidal structure with the WC_3 fragment acting as a metallacyclobutadiene π-bonded to the Fe(CO)$_3$ fragment as in Petit's classic compound (η^4-C$_4$H$_4$)Fe(CO)$_3$.[27] Although it is easy to qualitatively rationalize the asymmetry in the μ-C$_3$R$_3$ unit in Stone's compounds, in which first- and third-row transition-metal centers comprize the bimetallic template, it is at first somewhat perplexing to find the same asymmetry in the homo binuclear unit in this study. These observations can be reconciled by considering both the W(μ-C$_3$R$_3$)Fe- and the W$_2$(μ-C$_3$R$_3$)-containing compounds as isolobal analogues of Fe$_5$C(CO)$_{15}$,[28] having seven skeletal electron-bonding pairs and being predicted to exist as nido square-based pyramidal clusters. Because the loss of CO is presumably the rate-determining step in the reactions of the heterobinuclear complexes with alkynes, it may be that rate studies would provide little information about the C–C bond-forming process. One can speculate, however, that the essential features of the reaction mechanism subsequent to CO loss are similar to those observed for W$_2$(μ-CSiMe$_3$)$_2$ derivatives, vida infra.

A large group of trinuclear complexes bearing bridging acetylene ligands has been isolated[29] which is structurally related to the growing class of heterobinuclear complexes bridged by C$_3$R$_3$ ligands. The trinuclear species are, in most cases, square-based pyramidal molecules, having two metal centers and the two CR units of the acetylene ligand as the basal verticies of the pyramid. That both the MM'(μ-C$_3$R$_3$) dimers and the MM'M''(μ-C$_2$R$_2$) trinuclear molecules exist as nido clusters can be rationalized by demonstrating that differing vertices in the two species have an isolobal relationship. For example, Cp(CO)$_5$WFe[μ-C(Ph)C(*p*-tolyl)C(Ph)][26] and Cp$_2$(CO)$_7$W$_2$Os(μ-C$_2$Ph$_2$)[30] are both square-based pyramids because a three-electron donor μ-CR unit in the dinuclear complex is replaced by a three-electron donor Cp(CO)$_2$W unit in the latter compound.

In another related study,[31] alkynes were found to insert into the μ^3-CR ligand of (CO)$_9$(H)$_2$Ru$_3$(μ_3-CR) to produce a (μ^2-η^1,η^3-C$_3$,R$_3$) unit, bridging one face of the trinuclear cluster. A plausible step in the reaction of the trinuclear cluster with alkynes involves a M$_3$(μ^3-CR) $\rightleftharpoons$ M$_3$(μ^2-CR) equilibrium in which the μ_2-CR group is readily attacked by a coordinated alkyne during the C–C bond-forming step.

Certain features of the W$_2$C$_3$ core of the insertion products bear striking resemblances to Schrock's L$_3$W(η^2-C$_3$R$_3$) metallacyclobutadiene complexes,[32,33] which are prepared via the reaction of acetylenes with L$_3$W(CR) derivatives. Both **7a** and **10c** may be viewed as having a L'L$_2$W(C$_3$R$_3$) metallacyclobutadiene unit π-bonded to a d^2 L$_2$(L')W center (where L = CH$_2$SiMe$_3$ or *i*-PrO and L' = CSiMe$_3$). The symmetrical bond distances in the metallacyclobutadiene WC$_3$ fragment in **7a** can be equated with a similar arrangement found in Cl$_3$W[C(*t*-Bu)C(Me)C(Me)],[32] while the asymmetric distances in the WC$_3$ fragment of **10c** are more closely reflected by the bonding in Cp(Cl)$_2$W[C(Ph)C(*t*-Bu)C(Ph)].[33] The C$_3$R$_3$ ligands in Schrock's compounds also undergo facile rearrangements, apparently through reversible metallacyclobutadiene-to-metallatetrahedrane isomerizations. A significant difference in reactivity is observed for a class of (*t*-BuO)$_3$W(CR) complexes, in which the equilibrium between starting materials and metallacyclobutadiene products lies in favor of the starting materials. The reversible addition of alkynes to these alkoxide-substituted mononuclear derivatives allows them to act as alkyne metathesis catalysts. Studies of the L$_4$W$_2$(μ-CSiMe$_3$)$_2$ derivatives have uncovered no evidence that these species act as metathesis catalysts for alkynes.

There is current interest in the chemical reactivity of bridging hydrocarbon ligands.[34] Part of the impetus for this area of research originates in the modified chemical reactivity which bridging alkylidynes and alkylidenes display with respect to their terminal analogues. However, these studies are also of interest because μ-CR and μ-CR$_2$ moieties may represent soluble models for the reactive intermediates present in heterogeneous catalytic processes. The general applicability of μ^2-alkylidenes, which have been implicated as reactive intermediates in Fischer–Tropsch processes,[35] to C–C bond-forming reactions has been demonstrated by the reaction of olefins with (CO)$_8$Os$_2$(μ-CH$_2$) to form 1,2-dimetallacyclopentanes[36] and in the homogeneous oligomerization of alkynes by various complexes containing μ^2-alkylidene ligands.[37,38] Although bridging alkylidyne ligands have not benefited from such in-depth studies, they have also recently been identified as surface-bound species.[39,40] The discovery that olefins insert

(25) Jeffery, J. C.; Mead, K. A.; Razay, H.; Stone, F. G. A.; Went, M. J.; Woodward, P. C. *J. Chem. Soc., Chem. Commun.* **1981**, 867.
(26) Jeffery, J. C.; Mead, K. A.; Razay, H.; Stone, F. G. A.; Went, M. J.; Woodward, P. C. *J. Chem. Soc., Dalton Trans.* **1983**, 1383.
(27) Emmerson, G. F.; Watts, L.; Pettit, R. *J. Am. Chem. Soc.* **1965**, *87*, 131.
(28) Braye, E. H.; Dahl, L. F.; Hubel, W.; Wampler, D. L. *J. Am. Chem. Soc.* **1962**, *84*, 4633.
(29) Halet, J. F.; Saillard, J. Y.; Lissillour, R.; McGlinchey, M. J.; Jaoven, G. *Inorg. Chem.* **1985**, *24*, 218.
(30) Busetto, L.; Green, M.; Hessner, B.; Howard, J. A. K.; Jeffery, J. C.; Stone, F. G. A. *J. Chem. Soc., Dalton Trans.* **1983**, 519.
(31) Beanan, L. R.; Rahman, Z. A.; Keister, J. B. *Organometallics* **1983**, *2*, 1062.
(32) Pedersen, S. F.; Schrock, R. R.; Churchill, M. R.; Wasserman, H. J. *J. Am. Chem. Soc.* **1982**, *104*, 6808.
(33) Churchill, M. R.; Ziller, J. W.; McCullough, L.; Pedersen, S. F.; Schrock, R. R. *Organometallics* **1983**, *2*, 1046.
(34) Holton, J.; Lappert, M. F.; Pearce, R.; Yarrow, P. I. W. *Chem. Rev.* **1983**, *83*, 135.
(35) Van Barneveld, W. A. A.; Ponec, V. *J. Catal.* **1978**, *51*, 426.
(36) Motyl, K. M.; Norton, J. R.; Schauer, C. K.; Anderson, O. P. *J. Am. Chem. Soc.* **1982**, *104*, 7325.
(37) Levisalles, J.; Rudler, H.; Rose-Munch, F.; Daran, J. C.; Dromzee, Y.; Jeanin, Y.; Ades, D.; Fontanille, M. *J. Chem. Soc., Chem. Commun.* **1981**, 1055. *J. Organomet. Chem.* **1982**, *235*, C13.
(38) Adams, P. Q.; Davies, D. L.; Dyke, A. F.; Knox, S. A. R.; Mead, K. A.; Woodward, P. C. *J. Chem. Soc., Chem. Commun.* **1983**, 222.

into the alkylidyne C–H bond in $Cp_2(CO)_2Fe_2(\mu\text{-}CH)^+$, dubbed the "hydrocarbation reaction",[41] and that other C–C bond-forming reactions occur between μ-CR ligands and unsaturated hydrocarbons, vide infra, suggest that bridging alkylidyne ligands may be versatile agents for application in C–C bond formation and homologation.

Concluding Remarks. This study reveals that insertion into a bridging alkylidyne ligand in the reaction between alkynes and each of **1** and **2** proceeds via initial alkyne adduct formation, which is tantamount to an asymmetric oxidative addition to the dinuclear center. The two electrons involved in the M–M bond in **1** and **2** are transferred to the alkyne ligand which is counted as a 2– ligand. The subsequent insertion step is greatly influenced by steric factors, and the moderately large negative entropy of activation implies a highly ordered transition state. The formation of the μ-allyl ligand occurs by a direct C–C bond-forming process involving the least sterically substituted alkyne carbon, specifically *C*H for monosubstituted alkynes. Subsequent rearrangements within the μ-allyl ligand are relatively facile, and only when alkoxide ligands are present is the energy of activation for scrambling within the μ-C_3R_3 moiety greater than the energy of activation for insertion. The observed scrambling processes within the μ-$CR^1CR^2CR^3$ ligands can be adequately modeled by invoking a reversible rearrangement of the allyl ligand to a cyclopropenyl intermediate. The structural characterizations of the $W_2(\mu$-$C_3R_3)$-containing compounds reveal a marked preference for a ground-state structure having one tungsten atom contained within a tungstacyclobutadiene moiety which is in turn π-bonded to the other tungsten center. NMR studies reveal that a low-energy process interconverts the relative positions of the two tungsten centers, which implies a double minimum potential well.

Many questions are raised by this study. For example, why are the alkoxy-substituted μ-C_3R_3-containing compounds notably more sluggish toward scrambling within the μ-C_3R_3 ligand? Why does not a further reaction occur between alkynes and the μ-C_3R_3 insertion products? A reaction might involve either the remaining μ-$CSiMe_3$ ligand or the formed μ-C_3R_3 ligand. What electronic factors are important in controlling the insertion step and the thermodynamic stability of isomers for the μ-$CR^1CR^2CR^3$ ligands? Also, for rearrangements within the μ-C_3R_3 ligand, can an α/α' site exchange compete with a stepwise α/β and α'/β process? In our proposed scheme, Scheme II, this is equally possible on statistical grounds, but we have not in our experiments discovered a molecule where this is distinguished from successive α/β and α'/β site exchange. Despite these questions, the present work provides the first detailed study of the insertion of an alkyne into a μ-CR ligand at a dinuclear center.

Experimental Section

All reactions were carried out under a dry-nitrogen atmosphere by using standard Schlenk vacuum lines and glassware. Solvents were dried and deoxygenated by refluxing over Na/benzophenone except for ethanol and isopropyl alcohol, which were dried by refluxing over Mg turnings. NMR solvents were dried over 3-Å molecular sieves and were degassed by using a dry-nitrogen purge. Solid reagents were transferred in a Vacuum Atmospheres nitrogen-filled drybox. Acetylene derivatives were generally used as received; however, 1-phenyl-1-propyne was vacuum-distilled prior to use. Ethyne, propyne, and 2-butyne were measured and transferred as gases on a high-vacuum line. All liquid alkynes were measured and transferred via microsyringes. $W_2(\mu\text{-}CSiMe_3)_2(CH_2SiMe_3)_4$ was prepared according to the literature method.[5,6] Quantities up to 3 times that outlined in the original synthesis were prepared without significant loss of percent yield.

^1H and ^{13}C NMR spectra were obtained on a Nicolet 360-MHz spectrometer with 5000- and 34000-Hz spectral windows, respectively. ^1H NMR spectra were referenced against either the residual proton impurity in benzene-d_6 = 7.15 ppm or the residual proton impurity in the methyl group of toluene-d_8 = 2.09 ppm, while ^{13}C NMR spectra were referenced against either the carbon nuclei of benzene-d_6 = 128.0 ppm or the methyl group carbon nuclei of toluene-d_8 = 20.4 ppm. Infrared spectra were obtained as Nujol mulls between CsI plates by using a Perkin-Elmer 283 IR spectrophotometer. Mass spectra were obtained through the NSF Regional Mass Spectrometry facility at Lincoln, NE. Microanalyses were performed by Alfred Bernhardt Micro-analytische Laboratorium, West Germany, and all samples were ignited with V_2O_5 due to silicon content.

Preparation of Samples for Low-Temperature NMR Studies. All NMR samples used in low-temperature rate studies were prepared in the same manner. $W_2(\mu\text{-}CSiMe_3)_2(CH_2SiMe_3)_4$ (**1**) (0.050 g) was quantitatively transferred into a 5-mm thin-walled NMR tube in toluene-d_8 (0.54 g) (with $W_2(\mu\text{-}CSiMe_3)_2(O\text{-}i\text{-}Pr)_4$ (**2**), 0.040 g of material was used.) For low-boiling alkyne reactants such as ethyne, propyne, and 2-butyne, the solution in the tube was frozen at −196 °C, 1 equiv of alkyne was condensed above the frozen solution, and the tube was sealed under high vacuum. The samples were stored at −196 °C prior to use, at which time they were briefly thawed at temperatures between −70 and −50 °C and introduced into the precooled NMR probe. For high-boiling alkyne reactants, the NMR tube was capped with a 5-mm-i.d. serum cap. Just prior to use, the samples were cooled to −50 °C, and 1 equiv of alkyne was added through the serum cap via syringe. After brief agitation to ensure complete mixing, the samples were introduced into the precooled spectrometer probe. Significant polymerization occurred for NMR studies of the reaction of **1** with ethyne and propyne. For all other studies, however, the formtion of alkyne adducts and insertion products was apparently quantitative.

Synthesis of $W_2(\mu\text{-}CSiMe_3)_2(O\text{-}i\text{-}Pr)_4$ (2). **1** (1.0 mmol) was placed in a small reaction flask. Hexane (10 mL) and isopropyl alcohol (6.0 mmol) were added via syringe. The brown solution warmed immediately and acquired a yellow-green color over 6 h. After 12 h, the reaction mixture was filtered, the solvent was removed from the filtrate under vacuum, and the resulting green-brown residues were dissolved in a minimum of warm hexane. Following refrigeration at −20 °C, rodlike pale-green crystals (0.52 g) were isolated by filtration. The product was identified as $W_2(\mu\text{-}CSiMe_3)_2(O\text{-}i\text{-}Pr)_4$ (**2**) by ^1H and ^{13}C NMR spectroscopy and by elemental analysis: yield 67%; ^1H NMR δ 3.59 (4 H, sept, $J_{H\text{-}Me}$ = 5.8 Hz, OC*H*(Me)$_2$), 0.80 (24 H, d, $J_{H\text{-}Me}$ = 5.8 Hz, OCH(*Me*)$_2$), 0.62 (18 H, s, CSi*Me*$_3$); ^{13}C NMR δ 291.3 ($J_{^{183}W\text{-}^{13}C}$ = 140 Hz, *C*SiMe$_3$), 76.4 (*OC*H(Me)$_2$), 25.8 (OCH(*Me*)$_2$), 2.5 (CSi*Me*$_3$). Anal. Calcd for **2**: C, 31.0; H, 5.99. Found: C, 30.9; H, 5.91.

Synthesis of $W_2[\mu\text{-}C(H)C(SiMe_3)C(H)](\mu\text{-}CSiMe_3)(CH_2SiMe_3)_4$ (3a). **1** (0.50 mmol) was placed in a small reaction vessel equipped with a magnetic stir bar. Hexane (6 mL) was added to the flask via syringe, and the resulting brown solution was degassed and frozen at −196 °C. Ethyne (0.50 mmol) was condensed into the flask which was then sealed, immersed in a bath at −50 °C, and allowed to warm to ambient temperature with stirring over several hours. Filtration removed a small quantity of flocculent purple solid, presumed to be polyacetylene, leaving a clear brown filtrate. Removal of the solvent in vacuo allowed the recovery of a waxy brown solid (0.34 g) characterized as $W_2[\mu\text{-}C(H)C(SiMe_3)C(H)](\mu\text{-}CSiMe_3)(CH_2SiMe_3)_4$ (**3a**) by ^1H and ^{13}C NMR spectroscopy (Tables IV and V): yield 75%. Although the noncrystalline character of this compound precluded the collection of acceptable elemental analytical data, a mass spectrum of the sample displayed an envelope centered between 912 and 916 amu which is consistent with the proposed formula **3a**.

Low-Temperature NMR Studies of the Reaction of 1 with Ethyne. The reaction of ethyne with **1** was monitored by ^{13}C and ^1H NMR spectroscopy by using two samples prepared as described above. The sample for the ^{13}C NMR study contained ethyne-$^{13}C_2$ (92.5%), while the other sample contained unlabeled ethyne. At −78 °C, the ^1H and ^{13}C NMR spectra were consistent with the formation of the alkyne adduct $W_2(\mu\text{-}CSiMe_3)_2(CH_2SiMe_3)_4\cdot(C_2H_2)$ (**3b**) (Table VI). The $^{13}C\{^1H\}$ NMR spectrum showed a single carbon resonance at 216.8 ppm, consistent with the alkyne acting as a four-electron-donor ligand.[19] The ^{13}C NMR spectrum was the AA′ portion of an AA′XX′ pattern, having $^1J_{^{13}C\text{-}^{13}C}$ = 32.9 Hz. The ^1H NMR spectrum of **3b** had a single alkynic hydrogen resonance at 12.9 ppm. **3b** was stable over several hours at −30 °C.

Warming this sample to −10 °C allowed **3b** to convert to $W_2[\mu\text{-}C(H)C(H)C(SiMe_3)](\mu\text{-}CSiMe_3)(CH_2SiMe_3)_4$ (**3c**) with a $t_{1/2}$ of about 1 h. The ^1H NMR spectrum of **3c** at −10 °C showed two broad allylic hydrogen resonances at 9.26 and 5.89 ppm (Tables IV and V). The $^{13}C\{^1H\}$ NMR spectrum was consistent with this observation, showing two allylic carbon resonances at 135.8 and 153.3 ppm with a $^1J_{^{13}C\text{-}^{13}C}$ = 31 Hz (Table V). The allylic C–H units of **3c** clearly begin to exchange above −30 °C on the NMR time scale.

3c was rapidly converted to **3a** on warming to 15 °C. The ^1H and $^{13}C\{^1H\}$ NMR spectra of the final product were consistent with those obtained from a large-scale synthesis of **3a**. The ^{13}C NMR spectrum of **3a** appeared as the AA′ portion of an AA′XX′ pattern having a new $^2J_{^{13}C\text{-}^{13}C}$ = 11.5 Hz. No measurable change in the NMR spectrum of ^{13}C-labeled

(39) Kesmodel, L. L.; Dubois, L. H.; Somorjai, G. A. *Chem. Phys. Lett.* **1978**, *56*, 267.
(40) Koestner, R. J.; Frost, J. C.; Stair, P. C.; Van Hove, M. A.; Somorjai, G. A. *Surf. Sci.* **1982**, *116*, 85.
(41) Casey, C. P.; Fagan, P. J. *J. Am. Chem. Soc.* **1982**, *104*, 4950.

3a occurred at temperatures up to 85 °C.

Synthesis of $W_2[\mu\text{-}C(H)C(Me)C(SiMe_3)](\mu\text{-}CSiMe_3)(CH_2SiMe_3)_4$ (4a). **1** (0.50 mmol) was placed in a small reaction vessel equipped with a magnetic stir bar. Toluene (5 mL) was added via syringe, and the resulting solution was degassed and frozen at −196 °C. Propyne (0.50 mmol) was condensed into the flask which was then sealed, immersed in a bath at −78 °C, and allowed to warm to ambient temperature with stirring over 2 h. After filtration, the solvent was removed in vacuo and an orange–brown solid with properties similar to **3a** was isolated. The new compound was identified as $W_2[\mu\text{-}C(H)C(Me)C(SiMe_3)](\mu\text{-}CSiMe_3)(CH_2SiMe_3)_4$ (**4a**) by comparison of its ^1H and ^{13}C NMR spectra with those obtained for **3a** and **5a** (Tables IV and V). **4a** showed no evidence of allyl-group rearrangement on heating to 100 °C in solution and decomposed to uncharacterized products at higher temperatures.

Low-Temperature NMR Study of the Reaction of Propyne with 1. The reaction of **1** with propyne was monitored by ^1H NMR spectroscopy by using a sample prepared as described above. At −70 °C, the ^1H NMR spectrum of the sample was consistent with the formation of the alkyne adduct $W_2(\mu\text{-}CSiMe_3)_2(CH_2SiMe_3)_4\cdot[C_2(H)(Me)]$ (**4b**) (Table VI). The spectrum of the sample was examined at −50, −25, and 5 °C, showing no detectable change at these temperatures. As the temperature of the sample reached 10 °C, however, **4b** was converted to **4a** with a $t_{1/2}$ of approximately 30 min.

Synthesis of $W_2[\mu\text{-}C(Me)C(Me)C(SiMe_3)](\mu\text{-}CSiMe_3)(CH_2SiMe_3)_4$ (5a) and $W_2(\mu\text{-}CSiMe_3)_2(CH_2SiMe_3)_4\cdot(C_2Me_2)$ (5b). **1** (0.50 mmol) was placed in a small reaction vessel equipped with a magnetic stirrer. Hexane (7 mL) was added via syringe, and the resulting solution was degassed and frozen at −196 °C. 2-Butyne (0.50 mmol) was condensed into the flash which was then sealed and allowed to warm from −78 °C to ambient temperature over 2 h. Filtration of the reaction mixture and removal of solvent in vacuo allowed the recovery of a waxy brown solid material. The product was identified as $W_2(\mu\text{-}CSiMe_3)_2(CH_2SiMe_3)_4\text{-}(C_2Me_2)$ (**5b**) by ^1H and ^{13}C NMR spectroscopy at −40 °C (Table VI). A mass spectrum of this solid sample displayed an envelope centered around m/e 940, consistent with the suggested formula of **5b**. The addition of several equivalents of 2-butyne to **1** produced **5b** and a white solid material presumed to be an oligomer of 2-butyne. The ^1H NMR spectrum of **5b** at ambient temperature showed that a fluxional process allows the two (trimethylsilyl)methylidyne ligands to become equivalent on the NMR time scale. Raising the temperature of the sample to 40 °C in an effort to reach the fast-exchange limit caused the complete conversion of **5b** within minutes into the insertion product **5a**.

$W_2[\mu\text{-}C(Me)C(Me)C(SiMe_3)](\mu\text{-}CSiMe_3)(CH_2SiMe_3)_4$ (5a). **5a** was also produced when hexane and toluene solutions of **5b** stood at ambient temperature in excess of 10 days. **5a** is a brown soft-crystalline solid which was characterized by ^1H and ^{13}C NMR spectroscopy (Tables IV and V) and by elemental analysis. Anal. Calcd for **5a**: C, 35.7; H, 7.28. Found: C, 34.8; H, 6.63. ^1H and ^{13}C NMR spectra indicated that the C–Me groups of the allyl ligand in **5a** undergo site exchange on the NMR time scale. From ^1H NMR data: T_c = 55 °C, $\Delta\nu$ = 360 Hz, $\Delta G^{\dagger}_{calcd}$ = 14.9 ± 0.5 kcal/mol. **5a** was stable in solution at 100 °C over 30 min.

Kinetics of C_2Me_2 Insertion. The rate of insertion of the coordinated C_2Me_2 ligand in **5b** was studied via ^1H NMR spectroscopy. Bulk samples of **5b** were prepared and used in 0.050-mg quantities to prepare NMR samples as described above. The progress of the reaction was monitored by warming the samples to a set temperature for a measured time interval and then cooling the samples to −20 °C to directly compare the intensity of the alkynic methyl resonance of **5b** with the allylic methyl resonances of **5a**. Five data points covering three reaction half-lives were acquired for each rate study, and reaction rates were determined at four temperatures. All rate data conformed to simple first-order rate behavior, giving linear plots for ln [**5b**] vs. time, and relative rate constants were obtained from linear regression analyses. Relative rate constants: 40 °C, $k_r = 4.79 \times 10^{-5}$ s^{-1}; 50 °C, $k_r = 1.57 \times 10^{-4}$ s^{-1}; 65 °C, $k_r = 6.26 \times 10^{-4}$ s^{-1}; 80 °C, $k_r = 2.27 \times 10^{-3}$ s^{-1}. Activation parameters were obtained from these data using a ln (k_r time^{-1}) vs. T^{-1} plot and linear regression analysis: $\Delta H^{\dagger}$ = 20.5 ± 0.7 kcal/mol, $\Delta S^{\dagger}$ = −13 ± 2 eu.

Synthesis of $W_2[\mu\text{-}C(Me)C(Ph)C(SiMe_3)](\mu\text{-}CSiMe_3)(CH_2SiMe_3)_4$ (6a) and $W_2(\mu\text{-}CSiMe_3)_2(CH_2SiMe_3)_4\cdot[C_2(Me)(Ph)]$ (6b). **1** (0.44 mmol) and toluene (6 mL) were introduced into a small reaction vessel equipped with a magnetic stir bar. The flask was cooled to −60 °C, and 1-phenyl-1-propyne was added with stirring. After the solution was allowed to warm to −10 °C, the temperature was held between −10 and 10 °C for 2 h. Solvent was removed in vacuo to a volume of 0.2 mL, and the flask was placed in a refrigerator at −20 °C for several days. Removal of a thick mother liquor via syringe allowed the isolation of 0.21 g of sticky black crystals which were identified as $W_2(\mu\text{-}CSiMe_3)_2\text{-}(CH_2SiMe_3)_4\cdot[C_2(Me)(Ph)]$ (**6b**) by ^1H and ^{13}C NMR spectroscopy (Table VI): yield 48%. Warming samples of **6b** in toluene solution to 70 °C for several hours or allowing such samples to stand at ambient temperature over several days produced a brown noncrystalline product identified as $W_2[\mu\text{-}C(Me)C(Ph)C(SiMe_3)](\mu\text{-}SCiMe_3)(CH_2SiMe_3)_4$ (**6a**) by ^1H and ^{13}C NMR spectroscopy (Tables IV and V).

Synthesis of $W_2[\mu\text{-}C(Ph)C(Ph)C(SiMe_3)](\mu\text{-}CSiMe_3)(CH_2SiMe_3)_4$ (7a). **1** (0.50 mmol) and diphenylacetylene (0.50 mmol) were placed in a small reaction vessel equipped with a magnetic stir bar. Toluene (4 mL) was added via syringe, and the reaction mixture was allowed to stand at ambient temperature for 2 weeks. The solvent volume was reduced in vacuo, and black crystals were deposited from 0.2 mL of solution at −20 °C over 2 weeks. Removal of the mother liquor via syringe allowed the isolation of 0.21 g of material, identified as $W_2[\mu\text{-}C(Ph)C(Ph)C(SiMe_3)](\mu\text{-}CSiMe_3)(CH_2SiMe_3)_4$ (**7a**) by ^1H and ^{13}C NMR spectroscopy (Tables IV and V) and elemental analysis: yield 40%. Anal. Calcd for **7a**: C, 42.9; H, 6.77. Found: C, 42.7; H, 6.73. A sample of the product showed an envelope centered around m/e 1064 in the mass spectrometer which is consistent with the expected parent-ion envelope for **7a**. ^1H NMR spectra of reaction mixtures taken prior to complete formation of **7a** showed that **7a**, **1**, and diphenylacetylene are the only species present in significant concentrations in solution.

^1H NMR Study of the Reaction of 1 with C_2Ph_2. Three NMR samples containing **1** (0.070 g) were prepared as described above, except that varying amounts of C_2Ph_2 were added to each tube (for samples **a**, **b**, and **c**: 0.010, 0.100, and 0.350 g, respectively). After 8 h at 25 °C, the ^1H NMR spectrum of **c** showed resonances in the region between 3.0 and −1.0 ppm consistent with the conversion of **1** to $W_2(CH_2SiMe_3)_4(\mu\text{-}CSiMe_3)_2\cdot(C_2Ph_2)$, **7b** (Table VI). Sample **b** showed approximately 60% conversion of **1** to **7b**, while virtually no evidence of **7b** was detected in **a**. After an additional 2 days at 25 °C, **c** showed approximately 20% conversion of **7b** to the inserted product **7a**, while **b** contained only **7b** and 10–15% **7a**.

Synthesis of $W_2[\mu\text{-}C(Ph)C(H)C(SiMe_3)](\mu\text{-}CSiMe_3)(CH_2SiMe_3)_4$ (8a). **1** (0.30 mmol) was placed in a small reaction vessel equipped with a magnetic stir bar. Toluene (5 mL) was added via syringe, and, after the flask was cooled to −78 °C, phenylacetylene (0.30 mmol) was added with stirring. The reaction mixture was allowed to warm to ambient temperature over 2 h and was left to stir for 8 h. Removal of solvent in vacuo left an orange–brown noncrystalline solid. ^1H NMR spectroscopic studies at ambient temperature suggested that several products were present, but at −40 °C both ^1H and ^{13}C NMR spectra of the mixture allowed identification of the predominant isomer as $W_2[\mu\text{-}C(Ph)C(H)\text{-}C(SiMe_3)](\mu\text{-}CSiMe_3)(CH_2SiMe_3)_4$ (**8a**) (Tables IV and V). The allylic hydrogen resonances associated with **8a**, which appears at 9.57 ppm, broadened and diminished in intensity as the temperature of the sample was raised above −40 °C. At 10 °C, the resonance associated with **8a** was joined by another broad allylic hydrogen resonance at 6.08 ppm which probably represents $W_2[\mu\text{-}C(H)C(Ph)C(SiMe)_3](\mu\text{-}CSiMe_3)\text{-}(CH_2SiMe_3)_4$ (**8c**). In addition, a tiny sharp resonance was visible at 5.32 ppm, probably representing $W_2[\mu\text{-}C(H)C(SiMe_3)C(Ph)](\mu\text{-}CSiMe_3)\text{-}(CH_2SiMe_3)_4$ (**8d**). The allylic hydrogen resonances representing **8a** and **8c** broadened into the spectral base line by 55 °C, indicating that these isomers are capable of facile interconversion.

Low-Temperature NMR Study of the Reaction of 1 with $C_2(Ph)H$. The reaction of phenylacetylene with **1** was investigated via ^1H NMR spectroscopy when using a sample prepared as described above. At −40 °C, the ^1H NMR spectrum of the sample was consistent with the complete formation of the alkyne adduct $W_2(\mu\text{-}CSiMe_3)_2(CH_2SiMe_3)_4\cdot[C_2\text{-}(Ph)H]$ (**8b**) (Table VI). The coordinated phenylacetylene only began to insert at an appreciable rate at 15 °C. Both **8a** and **8c** appeared in equal quantities at this temperature, as is consistent with the observed facile interconversion of these isomers near ambient temperature.

Synthesis of $W_2[\mu\text{-}C(H)C(SiMe_3)C(SiMe_3)](\mu\text{-}CSiMe_3)(CH_2SiMe_3)_4$ (9a). **1** (0.50 mmol) was placed in a small reactor equipped with a magnetic stir bar. Toluene (5 mL) was added and, after the resulting solution was cooled to −78 °C, (trimethylsilyl)acetylene (0.50 mmol) was added with stirring. The reaction mixture was warmed slowly to ambient temperature and was filtered after 3 h. Reducing the solvent volume in vacuo, followed by refrigeration at −20 °C, produced 0.25 g of coal-black crystals. The new derivative was identified as $W_2[\mu\text{-}C(H)C(SiMe_3)C\text{-}(SiMe_3)](\mu\text{-}CSiMe_3)(CH_2SiMe_3)_4$ (**9a**) by ^1H and ^{13}C NMR spectroscopy (Tables IV and V) and elemental analysis: yield 50%. Anal. Calcd for **9a**: C, 35.4; H, 7.33. Found: C, 34.5; H, 6.90. Variable-temperature ^1H NMR spectroscopy revealed that two fluxional processes were occurring in **9a**. The first process involved hindered rotation about a C–Si bond in one of the allylic Me_3Si groups: $\Delta G^{\dagger}$ = 13 ± 1 kcal/mol. The second process involved the apparently simultaneous exchange of the allylic $(Me_3Si)C$ units and the two types of Me_3SiCH_2 ligands: $\Delta G^{\dagger}$ = 17 ± 1 kcal/mol.

Kinetics of $C_2(SiMe_3)H$ Insertion. The rate of insertion of a coordinated $C_2(SiMe_3)H$ ligand was studied via ^1H NMR spectroscopy with

samples prepared as described above. At −40 °C, the ^1H NMR spectra of all samples showed complete formation of the alkyne adduct $W_2(\mu\text{-}CSiMe_3)_2(CH_2SiMe_3)_4\cdot[C_2(SiMe_3)H]$ (**9b**) (Table VI). The progress of the reaction was monitored by warming the samples from −40 °C to a set temperature for a determined period of time, cooling the samples to −40 °C to halt the reaction, and then directly comparing the intensity of the coordinated alkynic hydrogen resonance of **9b** at 13.54 ppm with the allylic hydrogen resonance of **9a** at 6.63 ppm. Rate data and activation parameters were obtained by the methods described previously, vide infra. Relative rate constants: −30 °C, $k_r = 5.32 \times 10^{-5}$ s^{-1}; −20 °C, $k_r = 1.46 \times 10^{-4}$ s^{-1}; −12 °C, $k_r = 3.89 \times 10^{-4}$ s^{-1}; −5 °C, $k_r = 1.23 \times 10^{-3}$ s^{-1}; $\Delta H^{\ddagger} = 15.2 \pm 1.2$ kcal/mol; $\Delta S^{\ddagger} = -15 \pm 5$ eu.

Synthesis of $W_2[\mu\text{-}C(H)C(H)C(SiMe_3)](\mu\text{-}CSiMe_3)(O\text{-}i\text{-}Pr)_4$ (10c). **2** (1.0 mmol) was placed in a small reaction flask equipped with a magnetic stir bar. Hexane (10 mL) was added to the flask via syringe. The green solution was degassed and frozen at −196 °C, and ethyne (1.0 mmol) was condensed into the flask. The solution was warmed rapidly to ambient temperature with stirring and was filtered after 10 h. The solvent was removed from the filtrate in vacuo, and the resulting brown residue was dissolved in a minimum volume of warm hexane. Refrigeration at −20 °C followed by filtration yielded red-brown crystals (0.17 g) identified as $W_2[\mu\text{-}C(H)C(H)C(SiMe_3)](\mu\text{-}CSiMe_3)(O\text{-}i\text{-}Pr)_4$ (**10c**) by ^1H and ^{13}C NMR spectroscopy (Tables IV and V) and elemental analysis: yield 21%. Anal. Calcd for **10c**: C, 32.7; H, 5.94. Found: C, 32.5; H, 5.73.

Synthesis of $W_2[\mu\text{-}C(H)C(SiMe_3)C(H)](\mu\text{-}CSiMe_3)(O\text{-}i\text{-}Pr)_4$ (10a). **10c** (0.50 mmol) dissolved in toluene (10 mL) was warmed to 70 °C in a closed reaction vessel for 12 h. The solvent was removed in vacuo, and the resulting red-brown waxy solid was identified as $W_2[\mu\text{-}C(H)C(SiMe_3)C(H)](\mu\text{-}CSiMe_3)(O\text{-}i\text{-}Pr)_4$ (**10a**) by ^1H and ^{13}C NMR spectroscopy (Tables IV and V). **10a** was significantly more soluble in hexane and toluene than **10c** and, consequently, crystallized as sticky red-brown microcrystals at −20 °C from these solvents.

Reaction of 10c with Ethanol. **10c** (60 mg) was placed into a small Schlenk flask, hexane (5 mL) and ethanol (25 μL) were added via syringe, and the mixture was allowed to stand for 8 h at ambient temperature. The solvent and volatile products were removed in vacuo, and the entire sample was dissolved in benzene-d_6 and was analyzed via ^1H NMR spectroscopy. Three resonances representing the (trimethylsilyl)-methylidyne ligands of the three major products of the reaction appear near 0.5 ppm. Three resonances of similar intensity appearing near −0.1 ppm correspond to the $SiMe_3$ groups of the μ-$C(H)C(H)C(SiMe_3)$ ligand in these products. None of the products were directly identified due to the complexity of the ^1H NMR spectrum; however, it is assumed that they are isomers formed by partial substitution of the isopropoxide ligands by ethoxide ligands. It is particularly noteworthy that *no* resonances were observed near 0.4 ppm representing $SiMe_3$ groups in μ-$C(H)C(SiMe_3)C(H)$ rearrangement products.

Low-Temperature NMR Study of the Reaction of Ethyne with 2. The reaction of **2** with ethyne was monitored by ^{13}C NMR spectroscopy when using a sample containing **2** and ethyne-$^{13}C_2$ (92.5%), prepared as described above. The $^{13}C\{^1H\}$ NMR spectrum at −70 °C showed one carbon resonance at 187.3 ppm, consistent with the formation of the ethyne monoadduct $W_2(\mu\text{-}CSiMe_3)_2(O\text{-}i\text{-}Pr)_4\cdot(C_2H_2)$ (**10b**) (Table VI). The ^{13}C NMR spectrum of **10b** was the AA′ portion of an AA′XX′ pattern, having $^1J_{^{13}C\text{-}^{13}C} = 48.6$ Hz. A small amount of free ethyne-$^{13}C_2$ also remained at −70 °C, but this rapidly disappeared by the time the temperature reached −30 °C.

The entire sample of **10b** was converted into **10c** in the time necessary to bring the temperature of the NMR sample to −30 °C. The $^{13}C\{^1H\}$ NMR spectrum was consistent with that obtained from an authentic sample of **10c**, having two allylic carbon resonances at 178.9 and 113.3 ppm. A $^1J_{^{13}C\text{-}^{13}C} = 32.4$ Hz was also obtained from the ^{13}C-labeled sample (Table V). **10c** was stable over several hours of 10 °C.

Low-Temperature NMR Study of the Reaction of 2 with $C_2(SiMe_3)H$. The reaction of $C_2(SiMe_3)H$ with **2** was studied by ^1H NMR spectroscopy when using samples prepared as described above, except that **2** (0.050 g) and 1 equiv of $C_2(SiMe_3)H$ were used as reactants. The first sample showed no evidence of alkyne adduct formation when introduced into the spectrometer probe at −40 °C. When the temperature of the sample is raised to −20 °C, a compound whose ^1H NMR spectrum is consistent with the structure $W_2[\mu\text{-}C(SiMe_3)C(H)C(SiMe_3)](\mu\text{-}CSiMe_3)(O\text{-}i\text{-}Pr)_4$ (**11c**) appears with a $t_{1/2}$ of approximately 20 min (Table IV). While no evidence of a kinetically stable alkyne adduct **11b** was observed, a small singlet resonance at δ 9.57 may represent a low concentration of **11b** which is present during the insertion reaction. Warming the NMR sample containing **11c** to 80 °C for 1 min produces a rearranged derivative whose ^1H NMR spectrum is consistent with the structure $W_2[\mu\text{-}C(H)C(SiMe_3)C(SiMe_3)](\mu\text{-}CSiMe_3)(O\text{-}i\text{-}Pr)_4$ (**11a**) (Table IV).

A second ^1H NMR sample was used to monitor the rate of the reaction between $C_2(SiMe_3)H$ and **2**. The sample was introduced into the spectrometer probe at −50 °C and, after the accumulation of a spectrum at $t = 0$, was warmed to −25 °C to allow the reaction to proceed. The sample was cooled to −50 °C at intervals of 10, 20, 30, and 50 min to allow for data collection, and the extent of reaction was determined by comparing the intensity of the remaining free alkynic hydrogen resonance at 1.99 ppm with the residual hydrogen impurity in the methyl resonance of toluene-d_8 at 2.09 ppm. The reaction exhibited rate behavior far more consistent with a second-order rate law than the simple first-order rate behavior observed in previous studies, vide infra. Although it was evident that the data also showed some deviation from a simple second-order rate law, no further analysis of the data was undertaken.

Crossover Experiments. **7a** (0.50 mmol) was placed in a small reaction flask, and toluene (5 mL) was added via syringe. The resulting solution was degassed and frozen at −196 °C, and ethyne (0.50 mmol) was condensed into the flask. The flasks were sealed and immersed in a bath at −78 °C and allowed to warm to ambient temperature. On filtration and removal of solvent in vacuo, the brown solid residue was identified as **7a** by ^1H NMR spectroscopy. A sample of **5b** (0.50 mmol) was treated with ethyne under identical conditions with those described for the sample of **7a**. The brown solid residue isolated from this reaction was identified as **5b** by ^1H NMR spectroscopy.

Crystallographic Studies

General operating procedures and listing of programs have been previously given.[42]

$W_2(O\text{-}i\text{-}Pr)_4(\mu\text{-}CSiMe_3)_2$. The first few lovely green crystals examined tended to fracture (explode violently is a better term) when placed in the cold stream at −162 °C. For this reason, a suitable crystal was mounted and carefully cooled to −69 °C for characterization and data collection. There was no noticeable phase transition at this temperature, and the crystal seemed to behave properly during the course of data collection.

A systematic search of a limited hemisphere of reciprocal space located a set of diffraction maxima with no apparent symmetry or systematic absences, leading to the assignment of a triclinic lattice. Subsequent solution and refinement as well as statistical tests indicate the proper space group to be $P\bar{1}$.

The structure was solved by a combination of direct methods, Patterson techniques, and Fourier techniques. There are two independent molecules in the asymmetric unit, each lying at a crystallographic center. It is obvious from the data that the molecule is poorly behaved and lying near a phase transition. One of the molecules has a disordered isopropyl group, and, in general, all atoms are vibrating excessively. Considering the small size of the crystal and the poor quality of the data, no attempt was made to correct for absorption. Hydrogen atomms were included as fixed atom contributors except in the disordered part of the molecule.

$W_2(CH_2SiMe_3)_4(\mu\text{-}CSiMe_3)_2(\eta^2\text{-}PhCCMe)$. A suitable sample was cleaved from a larger crystal and affixed to a glass fiber by using silicone grease. The sample was then transferred to the goniostat where it was cooled to −157 °C for characterization and data collection.

A systematic search of a limited hemisphere of reciprocal space revealed a monoclinic lattice which could be indexed as $P2_1/a$. During data collection, 4 reflections, chosen as standards, were monitored after every 300 measurements. The standards continually decreased in intensity, and realignment did not bring them back to their original value. At the termination of data collection, the standards were between 20% and 40% lower in intensity. An anisotropic drift correction was therefore applied to the raw data during the data reduction process. Three nearly orthogonal reflections were used to apply the drift correction, and a third was used to check the results. The "test" reflection decreased in intensity by 35% prior to correction and 23% after correction, indicating that the correction was not entirely satisfactory.

The structure was solved by a combination of direct methods (MULTAN78) and Fourier techniques and refined by full-matrix least squares. Allowing the carbon and silicon atoms to vary anisotropically did not significantly lower the residuals, and several of the atoms converged to nonpositive-definite thermal parameters. For this reason, only the two tungsten atoms were assigned anisotropic thermal parameters in the final cycles. No attempt was made to include hydrogen contributions in the final model.

Examination of a final difference Fourier revealed eight peaks of intensity 1.1–2.3 e/Å^3 within 1.0 Å of the two tungsten atoms and one peak of intensity 3.2 e/Å^3 within 1.0 Å of the two tungsten atoms and one peak of intensity 3.2 e/Å$^+$ at coordinates 0.216, 0.007, 0.238. The latter could not be attributed to a "real" atomic position (lying ca. 1.1

(42) Chisholm, M. H.; Folting, K.; Huffman, J. C.; Kirkpatrick, C. C. *Inorg. Chem.* **1984**, *23*, 1021.

Table XVII. Summary of Crystal Data

	compound			
	2	**6b**	**7a**	**10c**
empirical form	$W_2Si_2C_{20}H_{46}O_4$	$W_2Si_6C_{33}H_{74}$	$W_2Si_6C_{38}H_{72}$	$W_2Si_2C_{22}H_{48}O_4$
color of cryst	green	black	black	red-orange
cryst dimensions, mm	0.08 × 0.08 × 0.10	0.06 × 0.12 × 0.13	0.08 × 0.08 × 0.11	0.07 × 0.16 × 0.20
space group	$P\bar{1}$	$P2_1/a$	$P2_12_12_1$	$P2_1/c$
cell dimensions				
temp, °C	−69	−157	−160	−158
a, Å	15.335 (4)	20.322 (13)	20.884 (9)	17.827 (7)
b, Å	11.515 (3)	12.344 (6)	13.734 (5)	17.872 (8)
c, Å	10.652 (3)	17.936 (10)	16.842 (6)	10.025 (3)
α, deg				
β, deg	122.52 (1)	91.16 (3)		106.07 (2)
γ, deg	99.96 (1)			
Z, molecules/cell	2	4	4	4
vol, Å^3	1550.34	4498.42	4830.57	3069.15
calcd density, g/cm^3	1.659	1.487	1.465	1.732
wavelength, Å	0.71069	0.71069	0.71069	0.71069
M_r	774.45	1007.16	1065.20	800.49
linear absorpt coeff, cm^{-1}	76.684	53.971	50.303	77.501
detector-to-sample dist, cm	22.5	22.5	22.5	22.5
sample-to-source dist, cm	23.5	23.5	23.5	23.5
av ω scan width at half height	0.25	0.25	0.25	0.25
scan speed, deg/min	4.0	4.0	4.0	4.0
scan width, deg + dispersion	2.0	2.0	2.0	1.8
individ background, s	6	8	8	8
aperture size, mm	3.0 × 4.0	3.0 × 4.0	3.0 × 4.0	3.0 × 4.0
2θ range, deg	6–45	6–45	6–45	6–45
tot no. of reflctns collected	6019	6855	6768	4590
no. of unique intensities	4057	5802	6120	4026
no. of $F > 3.00\sigma(F)$	3440	3045 (2.33σ)	5579	3348
$R(F)$	0.0660	0.0812	0.0521	0.0352
$R_w(F)$	0.0662	0.0829	0.0500	0.0357
goodness of fit for the last cycle	1.929	1.509	0.946	0.960
δ/σ for last cycle	0.05	0.05	0.05	0.05

Å from one of the W atoms) and thus must be an artifact of the poor quality of the data. Due to its position, one must view the distances and angles associated with atoms near the metals with caution.

Due to the poor quality of the data, no attempt was made to correct for absorption.

$W_2(CH_2SiMe_3)_4(\mu$-CSiMe$_3)(\mu$-C(Ph)C(Ph)CSiMe$_3)$. The crystal used for this study was cleaved from a larger crystal imbedded in a mass of crystals and contained one or two small fragments (each of less than 0.5 vol % of the primary crystal). The selected crystal was affixed to a glass fiber by using silicone grease and transferred to the goniostat where it was cooled to −160 °C. A systematic search of a limited hemisphere of reciprocal space revealed an orthorhombic cell with axial extinctions corresponding to $P2_12_12_1$.

Data were collected and processed in the usual manner, and the structure was easily solved by a combination of direct methods (MULTAN78) and Fourier techniques. After the completion of isotropic refinement, the correct enantiomorph was chosen for the crystal studied and a difference Fourier calculated to locate hydrogen atoms. While many of the hydrogen atoms appeared to be present, there were several spurious peaks which apparently interfered with their refinement. For this reason, hydrogens were included in the final cycles of refinement as fixed atom contributors, in idealized staggered positions.

ψ scans of several reflections were flat, and no absorption correction was performed. A final difference Fourier located numerous peaks of intensity 0.7–1.3 e/Å^3 throughout the cell.

$W_2(O$-i-Pr$)_4(\mu$-CSiMe$_3)(\mu$-C(H)C(H)CSiMe$_3)$. A suitable small crystal fragment was selected and transferred to the goniostat where it was cooled to −158 °C. A systematic search of a limited hemisphere of reciprocal space revealed a set of reflections which could be indexed as monoclinic, space group $P2_1/c$.

Data were collected by using the standard moving crystal—moving counter technique, and the structure was solved by heavy atom methods. The two W atoms were located by means of a Patterson function, and the remainder of the atoms were located in a difference Fourier phased with the W atoms. The data were corrected for absorption; see Table XVII. All atoms, including the H atoms, were refined by full-matrix least squares.

All non-hydrogen atoms were refined by using anisotropic thermal parameters, while the hydrogen atoms were treated with isotropic thermal parameters.

The final difference map was essentially featureless, the three largest peaks ranging from 0.83 to 1.9 e/Å and lying within 1.3 Å of the W positions. The two largest peaks were within 0.1 Å from the W atoms.

Acknowledgment. We thank the National Science Foundation, the donors of the Petroleum Research Fund, administered by the American Chemical Society, and the Wrubel Computing Center for support and Dr. Kirsten Folting for assistance in the crystallographic studies. We also thank Prof. C. P. Casey for stimulating discussions concerning the mechanism of alkyne insertion.

Registry No. 1, 96930-66-4; **2**, 96930-67-5; **3a**, 96930-68-6; **3b**, 96930-69-7; **3c**, 96998-67-3; **4a**, 96948-45-7; **4b**, 96930-70-0; **5a**, 96930-71-1; **5b**, 96930-72-2; **6a**, 96930-73-3; **6b**, 96948-46-8; **7a**, 96930-74-4; **7b**, 96948-47-9; **8a**, 96964-13-5; **8b**, 96930-75-5; **8c**, 96930-76-6; **8d**, 96930-77-7; **9a**, 96930-78-8; **9b**, 96930-79-9; **10a**, 96930-80-2; **10b**, 96948-48-0; **10c**, 96948-49-1; **11a**, 96930-81-3; **11b**, 96930-82-4; **11c**, 96930-83-5; ethyne, 74-86-2; polyacetylene, 25067-58-7; propyne, 74-99-7; polypropyne, 28391-48-2; 2-butyne, 503-17-3; 1-phenyl-1-propyne, 673-32-5; diphenylacetylene, 501-65-5; phenylacetylene, 536-74-3; (trimethylsilyl)acetylene, 1066-54-2.

Supplementary Material Available: Anisotropic thermal parameters, complete listings of bond distances and angles, and observed and calculated structure factors (48 pages). Ordering information is given on any current masthead page. The complete structure reports are available from the Indiana University Library in microfiche form only at a cost of $2.50 per report. For $W_2(O$-i-Pr$)_4(\mu$-CSiMe$_3)_2$ request MSC No. 84021, for $W_2(CH_2SiMe_3)_4(\mu$-CSiMe$_3)_2$(PhCCMe), MSC No. 83103, for $W_2(CH_2SiMe_3)_4(\mu$-CPhCPhCSiMe$_3)(\mu$-CSiMe$_3)$, MSC No. 83087, and for $W_2(O$-i-Pr$)_4$(CHCHCSiMe$_3)(\mu$-CSiMe$_3)$, MSC No. 84031.